TRANSPORTATION RESEARCH RECORD

549

Bituminous Mixtures, Aggregates, and Pavements

6 reports prepared for the 54th Annual Meeting of the Transportation Research Board

TRB

TRANSPORTATION RESEARCH BOARD

NATIONAL RESEARCH COUNCIL

Washington, D. C., 1975

Transportation Research Record 549
Price $3.00
Edited for TRB by Marjorie Moore

Subject areas
25 pavement design
31 bituminous materials and mixes
33 construction
35 mineral aggregates

The conference that is the subject of this report was approved by the Governing Board of the National Research Council acting in behalf of the National Academy of Sciences. Such approval reflects the Governing Board's judgment that the conference is of national importance and appropriate with respect to both the purposes and resources of the National Research Council.

The members of the committee selected to organize the conference and to supervise the preparation of this report were chosen for recognized scholarly competence and with due consideration for the balance of disciplines appropriate to the project.

Responsibility for the selection of the participants in the conference and for any summaries or recommendations in this report rests with that committee. The views expressed in individual papers and attributed to the authors of those papers are those of the authors and do not necessarily reflect the view of the committee, the Transportation Research Board, the National Academy of Sciences, or the sponsors of the project.

Each report issuing from such a conference of the National Research Council is reviewed by an independent group of qualified individuals according to procedures established and monitored by the Report Review Committee of the National Academy of Sciences. Distribution of the report is approved by the President of the Academy upon satisfactory completion of the review process.

LIBRARY OF CONGRESS CATALOGING IN PUBLICATION DATA

National Research Council. Transportation Research Board.
Bituminous mixtures, aggregates, and pavements.

(Transportation research record; 549)

1. Pavements, Bituminous—Design and construction—Congresses. 2. Bituminous materials—Congresses. 3. Aggregates (Building materials)—Congresses. I. Title. II. Series.
TE7.H5 No. 549 [TE270] 380.5'08s [625.8'5] 75-37616
ISBN 0-309-02454-4

FOREWORD

The papers in this RECORD may be grouped into two general areas. One group relates to theoretical models and techniques for estimating bituminous mix characteristics that are needed in rational flexible pavement design. These papers should be of interest to both the pavement designer and the testing engineer. The second group of articles deals with very practical problems of developing a method to preheat the base during cold-weather paving and of using spent oil shale as an aggregate in bituminous mixes.

The paper by Haas and Meyer presents an approach to developing cyclic creep models based on simulating field conditions in the laboratory. This model uses equipment that can apply dynamic stresses, under varying temperature conditions, and that measures accumulated pavement strains. The cyclic creep models, which can be used to separately estimate permanent deformation in the compression and tension areas of a bituminous layer, are described in detail. Very good agreement was found between predicted values of accumulated permanent deformation and actual values measured at the Brampton Test Road.

The dynamic modulus was the thrust of the work by Yeager and Wood. They developed a method for evaluating this modulus for Indiana state highway surface mixtures. The procedure incorporated variables such as stress level, cyclic loading rate, temperature, and asphalt type. In addition, the dynamic modulus of the bituminous paving mixture was correlated with a slope of the log kinematic viscosity versus 1 divided by the temperature plot, the cyclic loading rate, and the temperature of the test. The basic equation correlating these variables is given in the paper.

The fatigue behavior of slabs composed of three different dense bituminous mixes was investigated by Sharif by testing them under a constant-nonreverse stress type of loading. The effects of binder content, shape of coarse aggregate, rate of deformation, initial vertical deformation, and increase in its deflection with the number of cycles of fatigue life were investigated. Fatigue life was found to correlate very well with the initial deflection and increase in deflection combined. There are indications that a three-variable model is superior to a two-variable model as an estimating equation. Thus it was suggested that multiple linear regression equations should be used in such analyses.

The paper by Southgate and Deen is of special interest to the flexible pavement designers who are concerned with adjusting flexible pavement deflections to account for temperature variations. The authors used temperature data from widely scattered parts of the United States to develop basic techniques to account for variables such as altitude, latitude, longitude, and solar exposure in estimating the temperature at various depths in the pavement. The results are given in the form of linear regression equations and have a high degree of accuracy for the various locations checked.

A possible new source of aggregate, especially for construction in the Rocky Mountain area, may soon become available if oil shale is processed to obtain valuable hydrocarbon fuels. Gromko investigated the feasibility of using one spent shale aggregate in bituminous mixes. The results of the tests indicated that the spent shale aggregate is satisfactory for bituminous mixes except that it wears relatively easily. Mixes of the aggregate and asphalt were tested by the Hveem stabilometer and yielded high strength values.

Because many pavements that were undercompacted during cold-weather construction have failed, the paper by Shah and Dickson is especially timely. They developed a direct-fired propane heater for preheating the base for cold-weather paving. Their tests indicate that the method was quite feasible. After conducting tests, a graphical procedure was developed to predict the time available for compaction after the base was preheated. Estimates indicate that propane gas consumption for such a heater would cost approximately $138 per hour.

CONTENTS

CYCLIC CREEP OF BITUMINOUS MATERIALS UNDER TRANSIENT, HIGH-VOLUME LOADS

Ralph Haas and Frank Meyer, Department of Civil Engineering,
University of Waterloo, Ontario

Flexible pavements should be designed to limit the permanent deformation after a given number of load applications to some tolerable value. To accomplish this, the designer should be able to estimate the actual magnitude of permanent deformation for any particular design situation. The necessary predictive models for such cyclic creep should consider material characteristics; layer thicknesses; temperature; rate, intensity, and repetitions of loading; and any significant interactions of these factors. This paper presents an approach to developing cyclic creep models based on simulating field conditions in the laboratory. Equipment that can apply dynamic stresses under varying temperature conditions and that can measure accumulated permanent strains is described. The development of cyclic creep models that use data obtained from statistically designed experimental programs is described. They can be used to separately estimate permanent deformation in the compression and tension zones of a bituminous layer. The models were applied to the full-depth sections of the Brampton Test Road. Very good agreement was found between predicted and measured values of accumulated permanent deformation.

•EXCESSIVE permanent deformation of highway or airport pavements can accelerate structural deterioration and can create a safety hazard. This type of distress may well increase in the future because of the general trend toward increased traffic loads and volumes.

Pavement researchers have devoted considerable effort during the past few years to developing a working design technology for three major structural subsystems: fatigue, permanent deformation, and low-temperature shrinkage fracture. The permanent deformation subsystem is perhaps less advanced than the others. It requires the development of suitable models, so that the accumulation of permanent strains under transient, repeated wheel loads can be estimated.

The development of permanent strains, cyclic creep, depends on a variety of factors, including materials characteristics, layer thicknesses, temperature, rate of loading, and loading intensity and repetitions. A predictive model for cyclic creep should consider these factors and their interactions and should provide the pavement designer with a reliable estimate of permanent deformation as a function of time or traffic or both. He should be able to assess the effects of future traffic and the effects of various materials or layer thickness combinations for the particular design situation.

This paper describes a procedure for estimating cyclic creep in bituminous mixtures under transient, repeated load conditions. More specifically the objectives are

1. To outline the existing methodology for handling permanent deformation caused by cyclic creep in bituminous pavements,
2. To describe an approach based on laboratory simulation of field loading and environmental conditions and on the use of the experimental results in developing a predictive model,

Publication of this paper sponsored by Committee on Characteristics of Bituminous Paving Mixtures to Meet Structural Requirements.

3. To describe the effects of certain variables such as binder consistency and air voids content on the magnitude of cyclic creep, and
4. To briefly compare predicted and measured permanent deformation in the field.

PERMANENT DEFORMATION IN ASPHALT PAVEMENTS

Need for a Predictive Methodology

Excessive permanent deformation in bituminous pavements can result in distress, loss of serviceability, and loss of safety. A design methodology should be available to predict the actual magnitude of permanent deformation under any given situation. The importance of developing such a methodology has recently been emphasized by such forums as the Third International Conference on the Structural Design of Asphalt Pavements (1) and a Corps of Engineers-University of Texas conference (2).

The need for developing predictive techniques is reinforced by the following considerations.

1. With increasing wheel loads, tire pressures, and repetitions, the extrapolation of experience is risky.
2. Reducing shrinkage fracture potential by using softer asphalts may also increase the tendency for rutting during warm periods.
3. Rational design of pavements must include economic evaluation (including trade-offs); thus, it may at times be necessary to design to some tolerable level of permanent deformation.
4. Scarcity of resources may result in the economic feasibility of new materials; a fundamental, predictive technology is needed to assess their potential behavior.

Existing Methods

There are two current working methods, indirect in nature, that are used to design for permanent deformation. One provides minimum layer thicknesses and component material strengths, stability, density, or voids content; and the other limits the vertical compressive strain on the subgrade surface to some maximum level.

The first approach occurs inherently in the structural design method being used; the second was developed by the Shell Oil Company (3). Each is directed at precluding excessive permanent deformation, rather than predicting its actual magnitude.

The following more fundamental approaches have recently been suggested:

1. Quasi-elastic approach originally proposed by Klomp and Dorman (3) and extended by Romain (4),
2. Linear-viscoelastic approach developed by Moavenzadeh and coworkers at M.I.T. (5), and
3. Rut index approach developed by Barksdale (6).

The quasi-elastic approach is promising but requires development of certain deformation laws to become operational. The linear-viscoelastic approach was considered to be the most promising by the permanent deformation and materials characterization groups at an Austin, Texas, workshop in 1970 (7). However, this approach still has some significant limitations in its present state of development (8).

The procedure developed by Barksdale appears very encouraging in that it attempts to establish relationships from actual physical measurements.

A Simulation Approach

An approach that develops cyclic creep models from statistically designed experiments that simulate field conditions was reported initially by Morris and Haas (9, 10) and in subsequent detail by Morris et al. (11). It attempts to obtain relationships from measured data, in a manner somewhat similar to that of Barksdale (6), without presupposing any laws or properties. Also, through the use of statistically based experimental designs, the models can account for interactions of variables and can provide estimates of error.

To simulate field conditions requires that what occurs in a pavement subjected to a traffic load be known. Figure 1 shows the distribution of principal vertical σ_1 and horizontal σ_3 stresses throughout the depth of the upper layer (i.e., using a full-depth section, as shown in Figure 1a). At the same time, the temperature T in the slab might vary as shown in Figure 1c.

When a series of very short duration loads is placed on the pavement, as represented by moving traffic, the elements are subjected to stress pulses. These are shown in Figures 2a and b for σ_1 and σ_3 respectively. As well, a shearing stress occurs on the element as the load passes (Figure 2c).

Each element is also subjected to strains in the directions of the stresses. If these strains are completely recoverable, i.e., if the pavement rebounds to its exact original position after the load passes, then no permanent deformation will occur. However, there will usually be a very small portion of the strain that is not recoverable. After a large number of loads have passed over the pavement, the accumulation of very small irrecoverable strains can result in significant permanent deformation along the wheelpaths.

To completely simulate these responses in the laboratory is a highly complex problem and is essentially beyond the capabilities of current technology. However, they may be quite reasonably simulated by the use of a triaxial type of apparatus that can dynamically and independently apply σ_1 and σ_3 in either tension or compression with temperature control. The development and use of such an apparatus have been described in detail (10). A general view of the equipment is shown in Figure 3. It is capable of measuring cyclic creep, both axially and laterally, at any number of load applications.

EXPERIMENTAL PROGRAM

Materials and Testing Conditions

The material chosen for testing was the asphalt concrete base used at the Brampton Test Road in Ontario (12). It consists of a ¾-in. (19-mm) maximum size coarse aggregate, as shown by the grading curve in Figure 4. The asphalts used were 85/100 and 300/400 penetration grades. Their stiffness properties at various temperatures, plus viscosity at 275 F (135 C) and stiffness properties of the asphalt concrete, are given in Table 1. The 4 by 8-in. (102 by 203-mm) asphalt concrete samples were prepared in accordance with ASTM D 1561-71. Average air voids content of the samples was 7.1 percent, which compared very favorably with average field values of 7.2 percent.

The equipment used is shown in a general sense in Figure 3. A view of the asphalt concrete sample mounted on the base of the triaxial cell is shown in Figure 5.

The testing conditions essentially involved application of dynamic vertical and horizontal stress pulses, with intervening rest periods, to the samples shown in Figure 5. The duration of stress pulses was 0.04 sec, with a 0.02-sec rest period when the vertical stress was in the compressive mode and 0.21 sec when it was in the tensile mode.

Design of Experimental Program

The design of the experimental program was based on the premise that the amount of

Figure 1. Typical pavement stress and temperature distributions in center of wheelpaths under static loading.

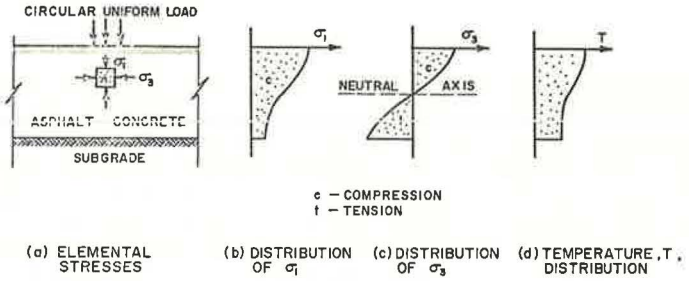

Figure 2. Stress variations in typical asphalt concrete element due to moving loads.

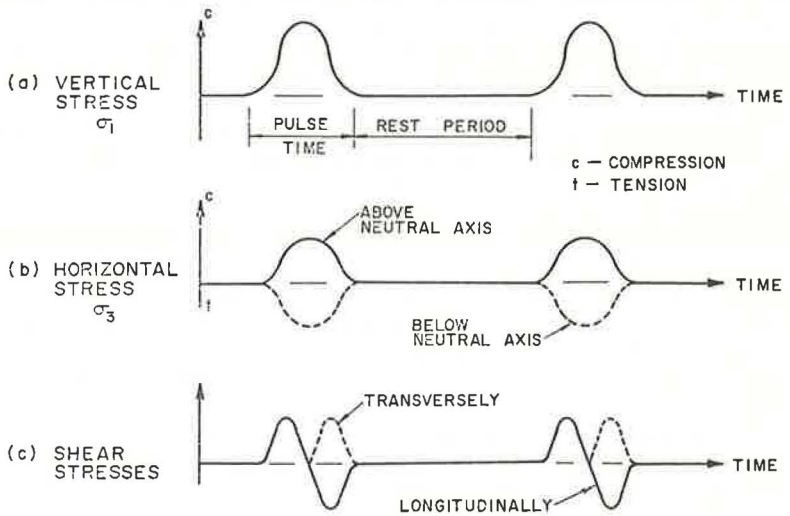

Figure 3. General view of equipment.

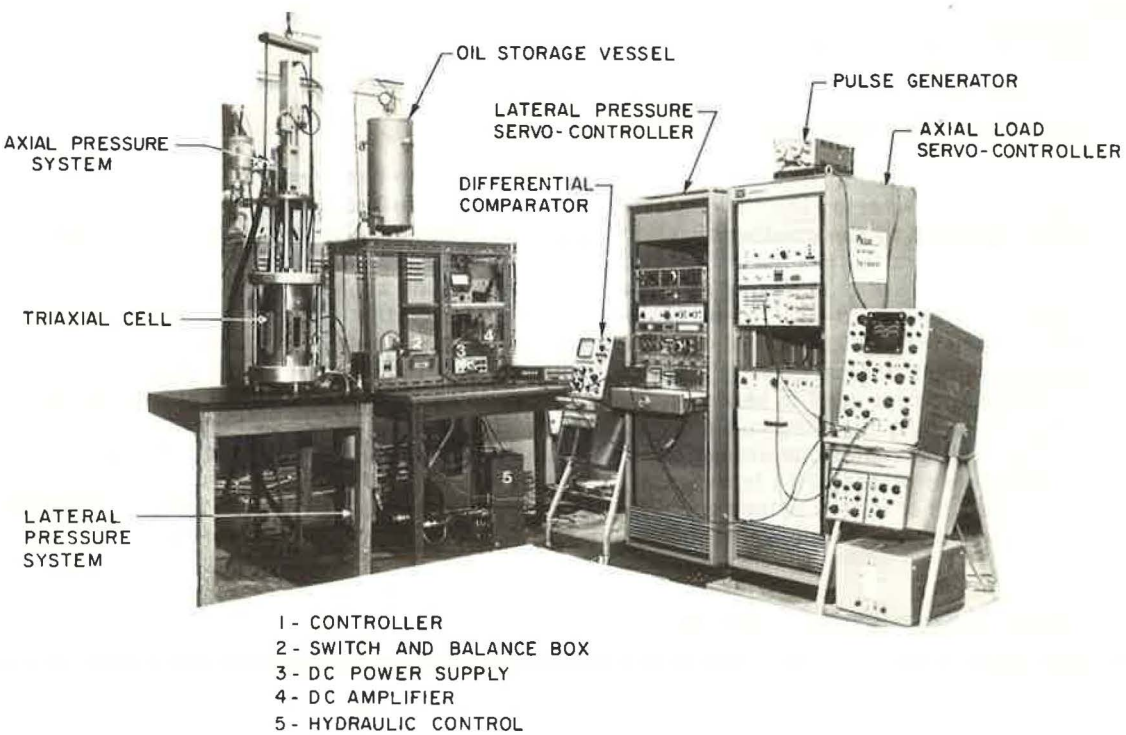

Figure 4. Average aggregate gradation curve of Brampton asphalt concrete base.

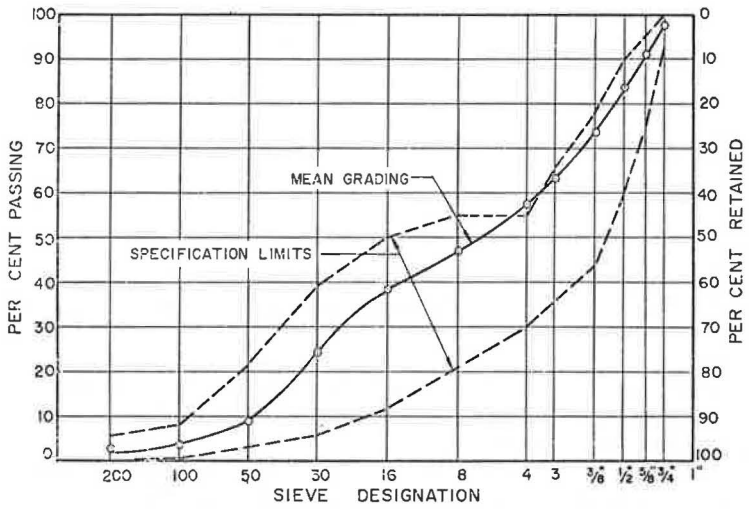

Figure 5. Lateral deformation transducers on specimen and heater.

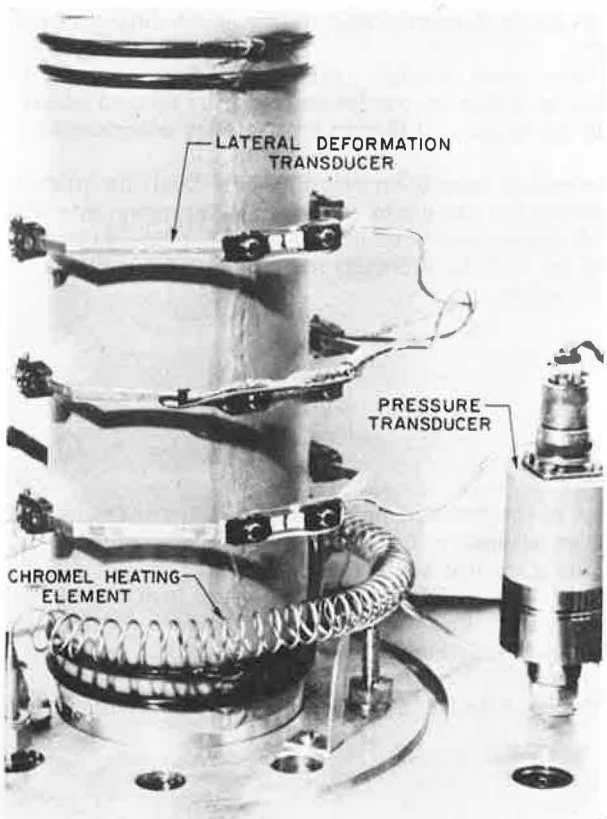

permanent strain, ϵ_p, in an element of asphalt concrete could be expressed in the following functional form:

$$\epsilon_p = f(\sigma_1, \sigma_3, T, N) \pm E \quad (1)$$

where

σ_1 = vertical stress,
σ_3 = horizontal stress,
T = temperature,
N = number of load repetitions, and
E = estimate of error associated with any attempt to predict ϵ_p as a function of the four factors listed.

Because it was suspected that the material might respond differently in tension than in compression (i.e., below the neutral axis of Figure 1), the program made provision for independently considering these two stress modes.

The experimental program consisted of factorial arrangements of variables in two phases. Phase 1 included a 2^3 factorial (i.e., three factors each at two levels) for the asphalt concrete with 85/100 penetration grade asphalt (Table 2). The factorial was replicated, and a composite design was included (to evaluate any possible interactions and quadratic or second order effects and to provide estimates of error).

Phase 2 included a 2^4 factorial for asphalt concrete with 85/100 penetration asphalt (tension series only) and 300/400 penetration asphalt (compression series only). The functional form was the same as given in Table 2, except that high and low levels of air voids were included as the fourth factor.

Phase 1 was conducted primarily to determine whether reliable relationships could be developed and to determine the existence of any major interactions or second order effects. Phase 2 was conducted to build air voids and binder consistency effects into the relationships.

The actual arrangements of these factorials have been described in detail by Morris (8) and by Meyer (13). The range of factors for the various factorial arrangements was 30 to 67 psi (207 to 462 kPa) for σ_1 in the compressive mode, 20 to 48 psi (138 to 331 kPa) for σ_1 in the tension mode, 15 to 86 psi (103 to 593 kPa) for σ_3, 60 to 93 F (16 to 34 C) for T, and 2.5 to 10 percent for air voids.

RESULTS

Tension and Compression Test Series

Figures 6 and 7 show typical test results in the form of permanent strain versus number of load repetitions. Figure 6 shows the relationship for a compressive series (σ_1 is compression), and Figure 7 shows that for a tensile series (σ_1 is tension).

In both cases, there is a conditioning phase for the first few thousand load repetitions, followed by a stable phase (i.e., a straight line increase of permanent strain with increasing numbers of loads). The slopes of the straight line portions of the relationships were used for the analysis of the results.

The data from phase 1 are given in Tables 3 and 4, and phase 2 data are given in Tables 5 and 6.

Development of Cyclic Creep Models

Mathematical models that are linear in the unknown parameters are widely used to relate

Table 1. Asphalt properties.

Asphalt Penetration	Penetration at 77 F	Viscosity at 275 F (stokes)	Stiffness of Asphalt Cement (psi)	Stiffness of Asphalt Concrete (ksi)
85/100	89	39	4,250	420
			1,420	225
			425	110
			142	70
300/400	297	18	426	100
			7,171	30
			14.2	10
			5.7	4

Note: 1 F = 1.8 C + 32; 1 stoke = 0.0001 m^2/s; 1 psi = 6890 Pa; 1 ksi = 6.9 Pa.

Table 2. Selected experimental program.

Axial Stress	Lateral Pressure	Temperature T_0	Temperature T_1
σ_1	σ_{30}	(1)	c
	σ_{31}	b	bc
σ_{11}	σ_{30}	a	ac
	σ_{31}	ab	abc

Note: Subscript 0 = low level, 1 = high level; a = σ_1; b = σ_3; c = T. Inclusion of code letter indicates that factor is at its high level.

Figure 6. Typical permanent strain, compression series.

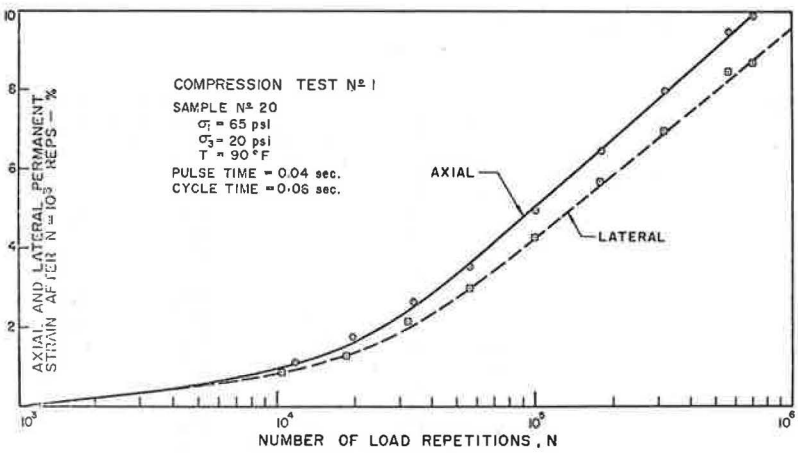

Figure 7. Axial and average lateral permanent strain, tension series.

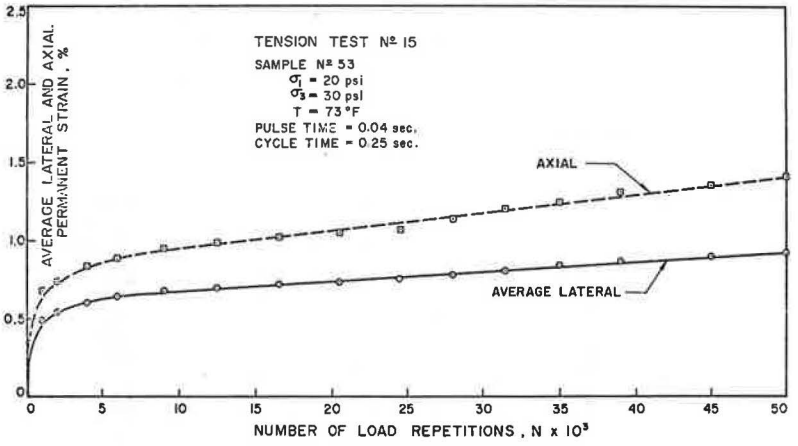

Table 3. Measured axial strain gradients/log N, compression series.

Item	Test No.	Sample No.	Condition	Gradient Percent/Log N
Main factorial	1	20	ac	5.80
	2	02	b	0.00
	3	38	c	3.10
	4	40	abc	0.10
	5	01	a	1.81
	6	23	a	0.56
	7	27	(1)	0.11
	8	26	ab	0.17
	9	42	b	0.10
	10	06	bc	-0.13
	11	09	c	1.50
	12	17	(1)	0.19
	13	08	abc	0.14
	14	14	ac	6.80
	15	44	bc	-0.27
	16	12	ab	0.05
Center and star points	17	34	σ_{10}	0.21
	18	30	Center	0.14
	19	33	Center	0.04
	20	36	T_1	0.16
	21	18	σ_{11}	0.15
	22	21	Center	0.11
	23	03	σ_{31}	0.07
	24	41	T_0	0.07
	25	07	σ_{30}	0.11

Note is as given in Table 2.

Table 4. Measured lateral strain gradients, tension series.

Item	Test No.	Sample No.	Condition	Gradient Percent/ 10^6 Cycles
Main factorial	1	59	abc	7.00
	2	69	b	0.38
	3	64	c	1.23
	4	61	c	2.10
	5	72	abc	6.58
	6	49	ac	0.63
	7	58	b	0.40
	8	50	(1)	0.20
	9	60	a	0.84
	10	47	ab	1.23
	11	74	a	1.36
	12	54	(1)	0.26
	13	48	ab	2.10
	14	55	bc	2.00
	15	53	bc	1.50
	16	45	ac	0.70
Center and star points	17	62	Center	1.60
	18	67	σ_{31}	2.14
	19	66	σ_{30}	1.00
	20	68	Center	1.74
	21	73	Center	1.40
	22	51	σ_{11}	2.60
	23	71	σ_{10}	0.47
	24	65	T_0	0.70
	25	56	T_1	2.90

Note is as given in Table 2.

Table 5. Tension results for 85/100 penetration asphalt.

Test No.	σ_v (psi)	σ_H (psi)	T (C)	Air Voids (percent)	Treatment	Percentage of ϵ_p per 10^5 Cycles
1	40	15	21	10	acd	2.1
2	20	35	16	10	bd	0.4
3	20	15	16	2.5	I	0.2
4	40	15	16	10	ad	1.35
5	40	35	21	10	abcd	9.75
6	20	35	16	2.5	b	0.6
7	40	15	16	2.5	a	1.0
8	20	15	21	10	cd	0.35
9	20	15	21	2.5	c	0.3
10	40	35	16	10	abd	2.0
11	40	35	16	2.5	ab	1.1
12	20	35	21	2.5	bc	0.4
13	20	35	21	10	bcd	2.1
14	20	15	16	10	d	0.2
15	40	15	21	2.5	ac	2.1
16	40	35	21	2.5	abc	2.2

Note: 1 psi = 6890 Pa.

variables such as those considered in this investigation. This requires the use of a number of assumptions, for purposes of simplification, as discussed by Davies (14), Yates (15), and others (8, 13).

If a good correlation between the outputs of the model and the observed data is not evident, a transformation may be necessary. Many such transformations are available, and several procedures can be found (16). In this investigation, a logarithmic transformation was satisfactory in phase 1 and phase 2.

The final models adopted from the analysis of data were as follows:

1. Compression mode, asphalt concrete with 85/100 penetration asphalt

$$\ln y = -1.7602 + 0.7\sigma_1 - 1.4281\sigma_3 + 0.4359T - 0.6790\sigma_3 T \quad (2)$$

where

y = predicted, accumulated permanent strain, in percent, per log number of load applications,
σ_1 = coded vertical stress [-1 for 45 psi (310 kPa) and +1 for 60 psi (414 kPa)],
σ_3 = coded lateral stress [-1 for 20 psi (138 kPa) and +1 for 80 psi (552 kPa)], and
T = coded temperature [-1 for 65 F (18 C) and +1 for 90 F (32 C)].

2. Tension mode, asphalt concrete with 85/100 penetration asphalt

$$\ln y = -0.1305 + 0.8404\sigma_3 + 0.3963T + 0.3261\sigma_1 + 0.2830AV + 0.2217AV\sigma_3 \quad (3)$$

where

y = predicted, accumulated permanent strain, in percent, per 10^5 load applications,
σ_1 = coded vertical stress [-1 for 20 psi (138 kPa) and +1 for 40 psi (276 kPa)],
σ_3 = coded lateral stress [-1 for 15 psi (103 kPa) and +1 for 40 psi (276 kPa)],
T = coded temperature [-1 for 60.8 F (16 C) and +1 for 69.8 F (21 C)], and
AV = coded air voids (-1 for 2.5 percent and +1 for 10 percent).

3. Compression mode, asphalt concrete with 300/400 penetration asphalt

$$\ln(y + 0.1) = -1.5424 + 0.6782\sigma_1 - 0.3472\sigma_3 + 0.2881AV - 0.2668\sigma_3 T - 0.2490\sigma_3 AV + 0.2286T + 0.2078\sigma_1 T - 0.1926\sigma_3 T\, AV + 0.1906\sigma_1 AV \quad (4)$$

where

y = predicted, accumulated permanent strain, in percent, per 10^6 load applications,
σ_1 = coded vertical stress [-1 for 30 psi (207 kPa) and +1 for 55 psi (379 kPa)],
σ_3 = coded lateral stress [-1 for 20 psi (138 kPa) and +1 for 35 psi (241 kPa)],
T = coded temperature [-1 for 64.4 F (18 C) and +1 for 78.8 F (26 C)], and
AV = coded air voids (-1 for 2.5 percent and +1 for 10 percent).

Equation 2 was derived from phase 1 in which air voids were not included as a variable; equations 3 and 4 come from the phase 2 results. The plausibility of these models was extensively evaluated in terms of lack of fit checks (8, 13). An examination of the residuals showed no patterns of inconsistency (i.e., the variances were relatively constant). Additionally, the standard error of the predicted value of y was about 0.89 for equation 2 and about 0.33 for equations 3 and 4 with an R^2 value of 0.94.

The models are reasonable in that an increase in y occurs for the following:

1. In tension, σ_1 increase, T increase, σ_3 increase, and AV increase; and
2. In compression, σ_1 increase, T increase, σ_3 decrease, and AV increase.

The models represented by equations 2 and 3 are relatively simple. Equation 4 is somewhat more complex, but this may be due to the effect of loading a material of lower stiffness (i.e., with softer asphalt). A tension model was not developed for the softer mix (with 300/400 penetration grade asphalt) because of the very low tensile stresses that would occur in a layer constructed with this material.

Field Comparisons

The basic steps required to predict permanent deformation in asphalt concrete pavements by using the models developed in this investigation are shown in Figure 8. The procedure is briefly detailed below.

1. Obtain the average temperature distribution throughout the asphalt concrete layer during those hours of the day when traffic is likely to cause permanent deformation. Depending on the degree of sophistication required and the sensitivity of the analysis, either a daily, weekly, or monthly average temperature may be selected.
2. Calculate the maximum vertical and horizontal stress distributions throughout the pavement at points immediately below the center of the wheelpaths. These can be reliably predicted by nonlinear elastic procedures such as finite element or iterative elastic multilayered solutions (18). The stiffness of the asphalt concrete is varied in accordance with the temperature distribution obtained in step 1.
3. Test the materials under simulated field conditions by using a statistically designed experimental program, and derive cyclic creep models of the form shown in Equation 1.
4. Calculate the total permanent deformation in the pavement after N load applications by dividing the layers into sublayers and summing the permanent deformations of the elements in each sublayer immediately below the center of the wheelpath. This can be expressed mathematically as

$$\Delta_p = \sum_{i=1}^{n} (\bar{\epsilon}_{pi})(\Delta_{hi}) \qquad (5)$$

where

Δ_p = total permanent deformation in the pavement system,
$\bar{\epsilon}_{pi}$ = average permanent strain in the ith sublayer,
Δ_{hi} = height (or thickness) of the ith sublayer, and
n = total number of sublayers in the pavement.

These steps were used to calculate the cumulative permanent deformations of the full-depth asphalt concrete sections at the Brampton Test Road. The following simplifying assumptions were made.

Table 6. Compression results for 300/400 penetration asphalt.

Test No.	σ_v (psi)	σ_H (psi)	T (C)	Air Voids (percent)	Treatment	Percentage of ϵ_p per 10^6 Cycles
1	55	20	26	2.5	ac	0.3
2	55	20	26	10	acd	4.5
3	55	35	26	2.5	abc	0.176
4	30	20	26	10	cd	0.2
5	55	35	18	2.5	ab	0.11
6	30	20	18	10	d	0.03
7	55	20	18	10	ad	0.3
8	30	35	26	10	bcd	-0.043
9	55	35	26	10	abcd	0.255
10	30	35	18	2.5	b	-0.004
11	30	20	18	2.5	I	0.011
12	55	35	18	10	abd	0.227
13	30	35	26	2.5	bc	-0.02
14	30	20	26	2.5	c	0.01
15	30	35	18	10	bd	-0.008
16	55	20	18	2.5	a	0.1

Note: 1 psi = 6890 Pa.

Figure 8. Basic steps in simulative statistically based approach.

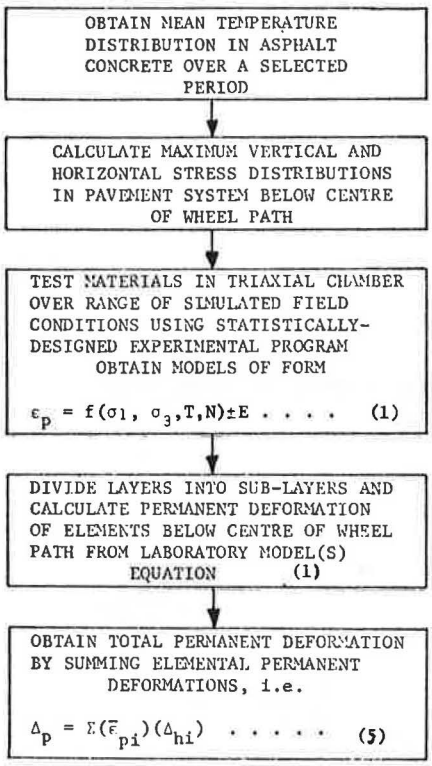

Figure 9. Average monthly pavement temperature-depth relationships.

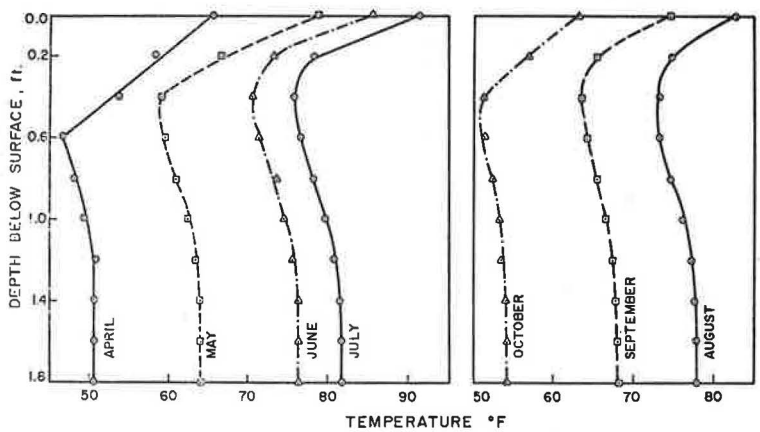

Figure 10. Vertical and horizontal stresses for 85/100 penetration full-depth asphalt concrete.

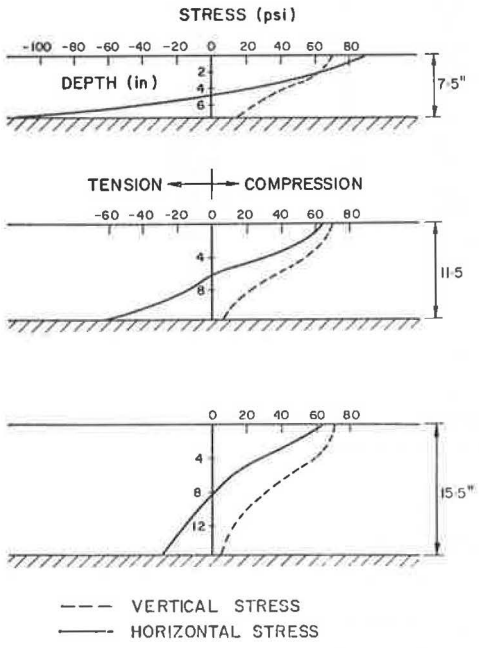

Figure 11. Vertical and horizontal stresses for 300/400 penetration full-depth asphalt concrete.

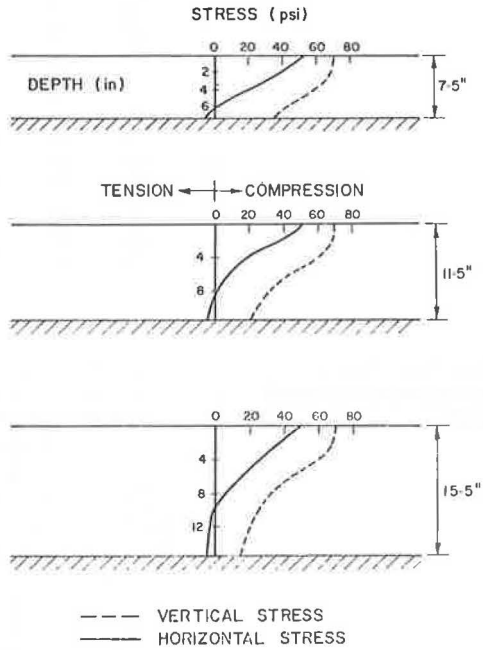

Figure 12. Rut depth-time relationship for section 3 of the Brampton Test Road.

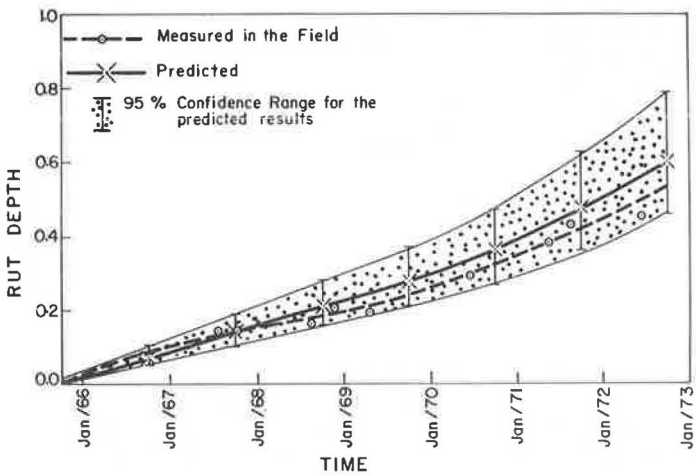

1. Traffic data—Classification surveys including counts have been conducted on the average four times annually since the test road was constructed. Axle weight studies have also been conducted, and data on the accumulated equivalent single axle loads have been obtained. The daily variation of these loads has been shown to be relatively constant, based on this data (8).

2. Pavement temperatures—These were analyzed by the Barber method (18). The average temperature and number of load repetitions should be calculated over that interval when permanent deformation is most likely to occur. This requires consideration of the truck traffic pattern, and the temperature below which little or no permanent deformation is likely to occur. A careful review of the Brampton data led to the assumptions that permanent deformation (a) occurs daily between 7:30 a.m. and 5:30 p.m., (b) occurs only in the period from April to October, and (c) can be ignored at temperatures below 50 F (10 C). Based on these assumptions, the average monthly temperature distributions shown in Figure 9 were obtained.

3. Stress analysis—Stresses were analyzed by means of a finite element program, FEPAVE II (20). The following assumptions were made: (a) The surface was stressed to 70 psi (482 kPa) uniformly over a circular area, 12.8 in. (322 mm) in diameter; (b) the temperature in the asphalt was distributed as shown in Figure 9; (c) the resilient modulus M_R of the subgrade was a function of the deviator stress σ_d as determined by repeated-load triaxial tests; (d) the stiffness-temperature relationship for the asphalt concrete was given by McLeod's indirect method (20) at a loading time of 0.04 sec; and (e) Poisson's ratio was 0.38 and 0.43 for the asphalt concrete and subgrade respectively. Typical stress distributions for full-depth sections 7.5, 11.5, and 15.5 in. (190.5, 292.1, and 393.7 mm) thick at Brampton for the maximum summer temperatures are shown in Figures 10 and 11 for mixes with 85/100 and 300/400 penetration grade asphalt (only the 7.5- and 11.5-in. thicknesses with 85/100 penetration grade were actually constructed; other values used are for comparative purposes).

The calculated values of accumulated permanent deformation for the 11.5-in.-thick section with 85/100 penetration grade asphalt are shown in Figure 12. Comparison with actual measured values, shown in the same figure, indicates a very good agreement. If a 300/400 penetration asphalt had been used in this section, the total accumulated permanent deformation would be estimated (using equation 4) at about 0.9 in. (23 mm).

A detailed examination of these results suggests that the major amount of permanent deformation in the harder asphalt layer actually occurs because of lateral flow in the tension zone (8), i.e., below the neutral axis.

CONCLUSIONS

The major points of this paper may be summarized as follows:

1. A reliable, predictive method for estimating cyclic creep in bituminous materials is a key aspect of a permanent deformation design subsystem.
2. An approach based on simulating field loading-temperature conditions in the laboratory is a practical way of developing cyclic creep models. The necessary equipment has been developed and briefly described in this paper.
3. Cyclic creep models of acceptable reliability have been developed by using a statistically designed experimental program. The models are relatively simple and they incorporate interactions of variables as well as estimates of error.
4. The models were able to predict permanent deformation for the full-depth sections at the Brampton Test Road in close agreement with actual measured values.

ACKNOWLEDGMENTS

Appreciation is extended to the Ministry of Transportation and Communications of

Ontario for cooperation in supplying information on the Brampton Test Road and for providing laboratory specimens.

REFERENCES

1. Proc., Third International Conference on the Structural Design of Asphalt Pavements. London, 1972.
2. Conference on Methods for Prediction of Permanent Deformations in Pavement Systems. Univ. of Texas at Austin, Aug. 1973.
3. A. G. J. Klomp and G. M. Dorman. Stress Distribution and Dynamic Testing in Relation to Road Design. Proc., Australian Road Research Board, 1964.
4. J. E. Romain. Rut Depth Prediction in Asphalt Pavements. Third International Conference on Structural Design of Asphalt Pavements, London, 1972.
5. F. Moavenzadeh, J. E. Soussou, and H. K. Findakly. Synthesis for Rational Design. Final Reports for FHWA Contract 7776, Vols. 1 and 2, Jan. 1974.
6. R. D. Barksdale. Rutting of Pavement Materials. Georgia Institute of Technology, Atlanta, Aug. 1973.
7. Structural Design of Asphalt Concrete Pavement Systems. HRB Special Rept. 126, 1970.
8. J. Morris. The Prediction of Permanent Deformation in Asphalt Concrete Pavements. Transport Group, University of Waterloo, Ontario, Sept. 1973.
9. J. Morris and R. C. G. Haas. Designing for Rutting in Asphalt Concrete Pavements. Presented at Annual Conference of Canadian Technical Asphalt Association, Vancouver, 1972.
10. J. Morris and R. C. G. Haas. Characterization of Bituminous Mixtures for Permanent Deformation Predictions. Presented at ASTM Annual Meeting, June 1973.
11. J. Morris, R. C. G. Haas, P. Reilly, and E. Hignell. Permanent Deformation in Asphalt Pavements Can Be Predicted. Presented at AAPT meeting, Feb. 1974.
12. R. C. G. Haas, N. I. Kamel, and J. Morris. Brampton Test Road: An Application of Layer Analysis to Pavement Design. Ministry of Transportation and Communications, Ontario, Rept. RR182, Nov. 1972.
13. F. R. P. Meyer. Permanent Deformation Prediction of Asphalt Concrete Pavements. M.A.Sc. thesis, Univ. of Waterloo, March 1974.
14. O. L. Davies. The Design and Analysis of Industrial Experiments. Oliver and Boyd, London, 1967.
15. F. Yates. Design and Analysis of Factorial Experiments. Imperial Bureau of Soil Science, London, 1937.
16. N. R. Proper and H. Smith. Applied Regression Analysis. John Wiley and Sons, New York, 1966.
17. R. D. Barksdale and R. G. Hicks. Material Characterization and Layered Theory for Use in Fatigue Analyses. HRB Special Rept. 140, 1973.
18. E. S. Barber. Calculation of Maximum Pavement Temperatures From Weather Reports. HRB Bulletin 168, 1957.
19. J. M. Duncan, C. L. Monismith, and E. L. Wilson. Finite Element Analysis of Pavements. Highway Research Record 228, 1968.
20. R. C. G. Haas. A Method for Designing Asphalt Pavements to Minimize Low-Temperature Shrinkage Cracking. Asphalt Institute, Rept. 73-1, Jan. 1973.

FATIGUE BEHAVIOR OF CONVENTIONAL AND RATIONALLY DESIGNED BITUMINOUS MIXES ON SIMULATED SUBGRADE

R. L. Sharif, Ministry of Public Works, Amman, Jordan

Three dense bituminous mixes were designed by a method that takes into consideration the shape, size, size distribution, and surface texture of mineral aggregates and boundary condition of the mold. Laboratory investigation into the fatigue properties of these mixes was carried out on slab specimens having a thickness of the same order of the wearing course. A simulated subgrade, based on the Westergaard assumption, was designed to support the slab specimens subjected to a constant nonreversed stress type of loading. The effect of variables such as the binder content, shape of coarse aggregate, rate of deformation, and initial vertical deflection on the fatigue life of slab specimens was investigated. Life of the mixes can be predicted from either the initial deflection of the specimen, the rate of increase in this deflection, or both. Fatigue life correlated very well with these two variables combined. The experimental results showed that the fatigue strength of the three rationally designed mixes was superior to that of the B. S. 594 wearing course mix made of the same type of stone.

•DESIGN of a bituminous mix should take into consideration not only rutting, plastic flow, Marshall stability, durability, and skid resistance but also fatigue cracking (1, 2, 3, 4).

There is a great need for detailed information on the bending characteristics of bituminous mixes, their fatigue behavior, and the effect of many variables on this behavior (5, 6, 7, 8).

To gain knowledge on the fatigue behavior of bituminous mixes, a laboratory investigation was carried out on four mixes to determine the effect of variables such as binder content, shape of coarse aggregate, and rate of vertical deflection on their fatigue behavior and to establish the relative merits of these mixes against the conventional British Standard 594 rolled asphalt wearing course mix.

TEST AND MODE OF LOADING

Previous researchers mainly used either controlled stress (9) or controlled strain (7) loading conditions. Some few, however, employed constant deflection loading conditions (10).

Some researchers applied the stress or strain as reversed or partially reversed to limit the magnitude of accumulated deformation in the viscoelastic materials; others did not reverse the loading conditions.

Some researchers supported tested beams (10) or slab specimens (11, 12, 13) on springs to simulate, to some extent, actual road conditions or worked directly on tracks (9). Others dealt with the more fundamental approach to the problem and worked on cylindrical and beam specimens without any simulation.

Publication of this paper sponsored by Committee on Characteristics of Bituminous Paving Mixtures to Meet Structural Requirements.

In summary, there have been many variations in the type of tests, mode of loading, and shape of specimens used. All of these variations have a great influence on the fatigue behavior of the bituminous mix, and they present a great deal of difficulty in interpreting the results.

It is believed, however, that this difficulty can, to some extent, be decreased and controlled if a test that simulates actual road conditions is used. With this in mind, a slab specimen prepared in a realistic way (rolling), having a thickness of the same order of the wearing course, simply supported by a simulative subgrade, and subjected to constant repeated loading was conceived.

This type of test has the following advantages:

1. Provides an improvement over cylindrical specimens whose preparation or testing is far from realistic;
2. Provides an improvement over beams tested with unidirectional bending by allowing plane bending in the slab;
3. Reveals the effect of mix and test variables in the most realistic way;
4. Allows the mixes to be compared and arrayed in roughly the same order both in the laboratory and on the road; and
5. Yields considerable information on the likely performance of that mix on the road.

DESIGN OF SIMULATED SUBGRADE

In analyzing stresses in a rigid pavement, Westergaard (14) considered the subgrade to be a discontinuous medium (similar in action to a mesh of closely spaced springs) in which the vertical deflection at any point is proportional to the pressure at that point and independent of pressure elsewhere. Burmister (15), on the other hand, assumed the subgrade to be an elastic solid that is completely continuous.

Inasmuch as the major portion of elastic deflection on the road was found to occur in the subgrade, many researchers assumed its behavior to be elastic, and they simulated it with steel compression springs (Winkler support) over which they laid the bituminous beam or slab specimens (4, 11). The results with this type of subgrade were easier to interpret than those with Burmister's type of subgrade.

Based on this information, a similar approach was adopted for this research, and a simulated subgrade was designed.

Compression springs, 150 mm long and 25 mm in diameter, that deflect 25 mm under a load of 250 kg were used. To install the springs, half-depth, 25-mm-diameter holes were drilled in a steel plate measuring 800 by 500 by 50 mm and spaced at 65-mm centers in both the longitudinal and transverse directions. The springs were fitted into these holes and were kept upright and prevented from lateral movement by means of a 25-mm-deep steel grid having 26.5-mm-square openings (a clearance of 1.5 mm was allowed for each spring).

Each spring is covered by 50-mm-square by 12.5-mm steel plates bearing on 15-mm-diameter balls to allow for the free movement of these plates. This movement was intended to keep the plates in contact with the bituminous slab resting on them during the deflection of the slab under the action of the load. The keying or stress concentration likely to be produced by fixed top plates was thereby eliminated.

LOADED AREA AND TESTING MACHINE

Specimens were tested by the Instron machine while simply supported on the simulated subgrade. The load was applied by a 75-mm-diameter steel disk faced with a thin piece of solid rubber.

To ensure that the behavior in the horizontal direction of the slab would be as infinite as possible, the slab thickness and the plunger area were chosen to be the practical minimum, the stiffness ratio between the slab and the support was kept low, and the

testing temperature was relatively high (around 20 C).

MIXES AND SPECIMENS

Four mixes of gritstone (as coarse aggregate), leighton buzzard sands (as fines), portland cement (as a filler), and 50/60 penetration binder were prepared in 450 by 450 by 50-mm slab specimens at four binder contents each (6, 7, 8, and 9 percent by weight of aggregates). A total of 64 specimens were prepared.

Each specimen while confined in the slab mold was subjected to twelve 1-metric ton roller passes.

The first three mixes were designed to the rational method of mix design (16) that takes into consideration the shape, size, size distribution, and surface texture of mineral aggregates and boundary condition of the mold.

The top three sizes of the coarse aggregates (18, 12, and 9 mm) were not sorted by shape (as produced) in the first mix (mix O), flaky in the second mix (mix F), and non-flaky in the third mix (mix q).

The resulting gradings of these mixes and of the B. S. 594 specification are given in Table 1.

FATIGUE TEST AND RESULTS

In the test, the slab was placed on the top of the simulated subgrade, and a central load of 70 kg was applied repeatedly by the Instron plunger moving at a 3-cm/min rate of deformation. A dial gauge was mounted just beside the edge of the plunger to record the vertical instantaneous elastic deformation and the cumulative permanent deformation.

The test was carried out at room temperature, which varied from 19 to 23 C. The four mixes were tested at each binder content in an order that minimized the effect of temperature variations on fatigue life.

Each specimen was subjected to 10 load cycles so that it could embed itself into the top plate. Then, the effect of rate of deformation on the deflection of the slab was investigated by subjecting each specimen to the following cycle rates: 5, 3, 2, 1, 0.5, 0.3, 0.2, and 0.1 cm/min. Subsequently, a 3-cm/min rate was applied repeatedly until failure.

FAILURE CRITERION

In this type of test, the slab did not fracture completely but continued to act as an intact specimen under the load for a very long time.

Figure 1 shows a typical trace of the permanent deformation per cycle, the cumulative permanent deformation, and the instantaneous elastic deformation of a slab specimen. The two curves of elastic deformation are parallel, but the former exhibits higher values than the latter. This is mainly because the chart records the instantaneous elastic and plastic deformations in the slab together with the deformation in the rubber pad and the instantaneous compaction in the slab area under the piston. The dial gauge, on the other hand, records in a single reading the instantaneous elastic deformations only.

The elastic deformation in both cases shows a continuous gradual increase with the increase in the number of cycles; other researchers (17) found that the elastic deformation was constant.

As can be seen in Figure 1 the elastic deformation and the cumulative permanent deformation curves follow one general trend: During the first few cycles, the plots show a rapid initial increase in the deflection mainly because of the embedment of the slab in the top plates. Afterward, the plots start out as straight lines having very small rates of increase in deflection with an increase in the number of cycles. At some state

Table 1. Gradings of mixes (percentage by weight).

Sieve Size	Mix O	F	q	B.S. 594
3/4 in.	100	100	100	100
1/2 in.	95.4	96.4	94.4	98
3/8 in.	88.6	92.3	87.4	84
1/4 in.	78.4	84.1	75.8	67
No. 7	68.5	73.5	65.9	67
No. 14	48.8	53.5	44.9	64
No. 25	39	41.2	35.5	58
No. 52	27.9	28.5	25.7	41
No. 100	17.5	16.1	16.4	22
No. 200	8.2	7.1	8.1	8.5

Note: 1 in. = 25.4 mm.

Figure 1. Vertical deflection versus number of load repetitions.

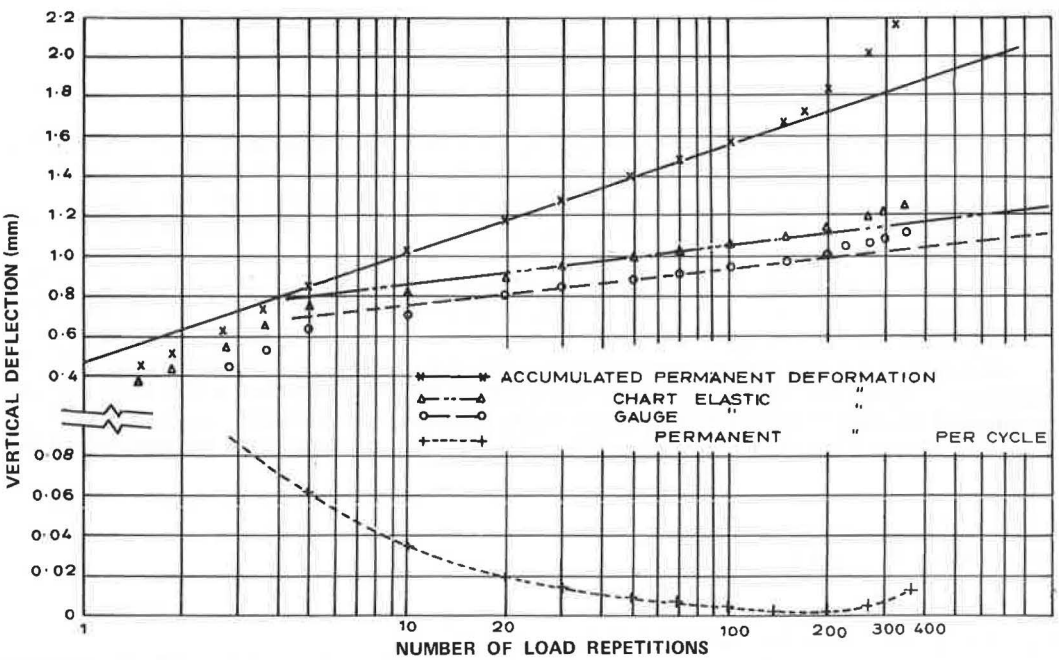

the plots show a deviation upward from the straight lines.

The permanent deformation curve, on the other hand, is different from the other three curves. It shows a very large deformation at the beginning and decreases continuously until it reaches a minimum, where it starts to increase again very slowly.

The permanent deformation curve reaches its minimum at roughly the point at which the other three curves deviate from the straight line. This is considered the failure point of the slab.

A close examination of the underside of the slab after failure showed that dry slabs had cracks similar to the surface alligator cracking observed in actual pavements (6). The rich slabs, on the other hand, did not show these cracks although their curves deviated from the straight line.

CYCLES VERSUS BINDER CONTENT

Results of the average values of the number of cycles to failure of the four mixes are shown plotted against binder content in Figure 2. In that figure, each mix shows a peak value of fatigue life, the maximum exhibited by mix O followed by mix F, B.S. 594, and mix q at 7.2, 7.2, 7.7, and 7.5 percent OBCs respectively. The OBC of mix q appears to be the least critical, which suggests that fatigue life of this mix would not vary much if the binder content was changed well above or below the OBC in order to satisfy other requirements.

Moreover, the fatigue life of B.S. 594 mix is well below that of any of the other mixes at low binder contents. At high binder contents, however, the difference was considerably reduced, suggesting that dry mixes depend more on their interlocking structure in their response to the load. Accordingly, continuously graded mixes (O, F, q) should exhibit higher fatigue life than the gap-graded B.S. 594 mix. At high binder contents, on the other hand, the particles were pushed away (dilated) by the excess binder (above the OBC), and their interlock was reduced. At this stage the four mixes became very similar, consisting mainly of a matrix with stone particles dispersed therein.

That mix F exhibited higher life than both mix q and the B.S. 594 would indicate that flaky particles improved the fatigue life. The propagation of cracks is more frequently through the particles in the flaky mix and around them in the nonflaky mix.

Mix F, however, is still exhibiting lower fatigue life than mix O, indicating that flakiness of the particles benefits life up to a certain limit, beyond which this flakiness might become harmful. Economically, using a limited amount of flaky particles in a bituminous mix would mean fewer restrictions on aggregates incorporating them, and nonflaky particles could be saved for jobs that need them most (e.g., surface dressings).

INCREASE AND RATE OF DEFORMATION OF ELASTIC DEFLECTION

The initial elastic deflection of the specimen is read from the dial gauge elastic curve at the 50th cycle (Figure 1) after the slab has embedded itself into the support. The slope of the straight portion of this curve is the rate of increase in the elastic deflection with the number of cycles. The rate of deformation is the vertical speed of the cross head of the Instron machine.

Average values of the initial vertical deflections in the slab at the 50th cycle (70-kg load at a 3-cm/min rate of deformation) and the increase in deflection per 100 cycles for all the mixes are shown plotted against binder content in Figures 3 and 4.

In Figure 3, each mix shows a minimum value of initial vertical deflection, the lowest of which is exhibited by mix q followed by mixes O, F, and B.S. 594 at 7.3, 7.5, 7.4, and 7.5 percent OBCs respectively.

Figure 4 shows a minimum value of increase in vertical deflection for each mix; the lowest minimum was exhibited by mix F followed by mixes q, O, and B.S. 594 at 7.6, 7.2, 7.3, and 7.7 percent OBCs.

Figure 2. Number of load repetitions to failure versus binder content.

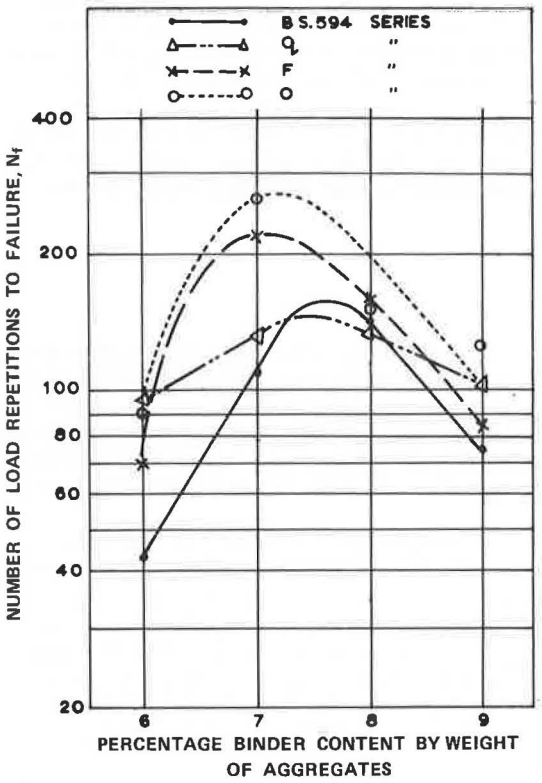

Figure 3. Initial vertical deflection versus binder content.

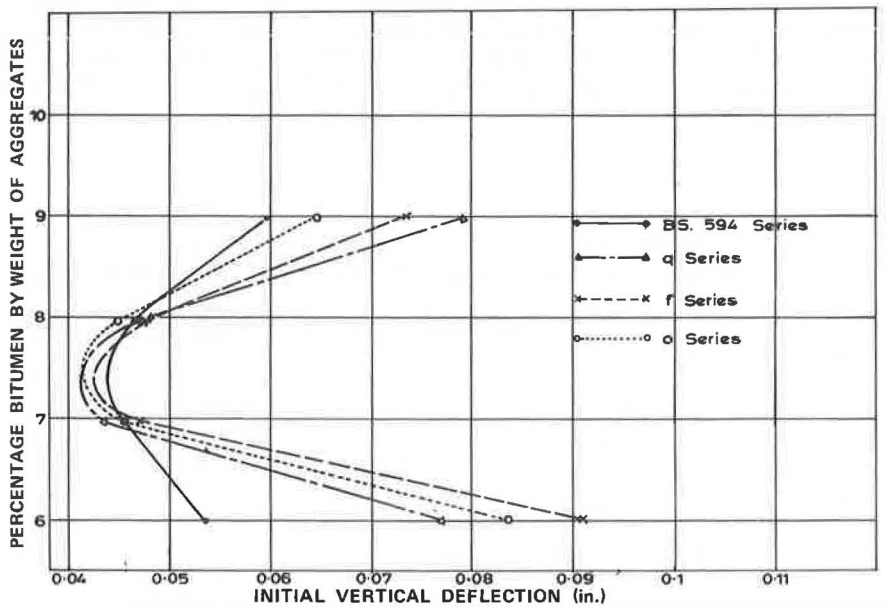

Figure 4. Rate of increase in vertical deflection versus binder content.

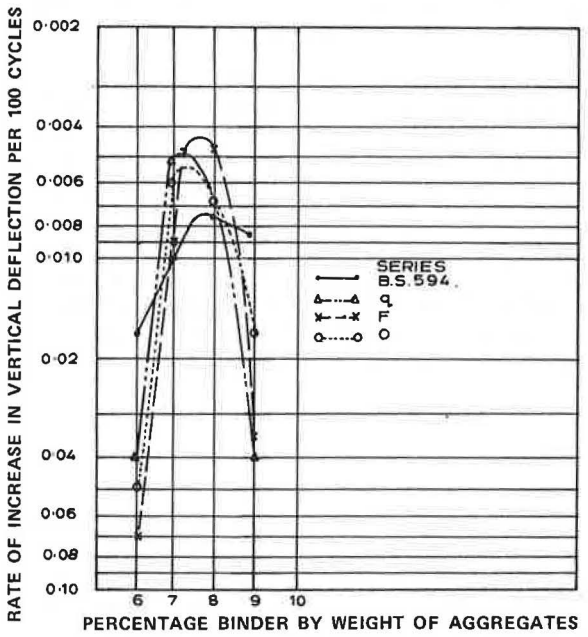

Figure 5. Number of load applications to failure versus initial vertical deflection.

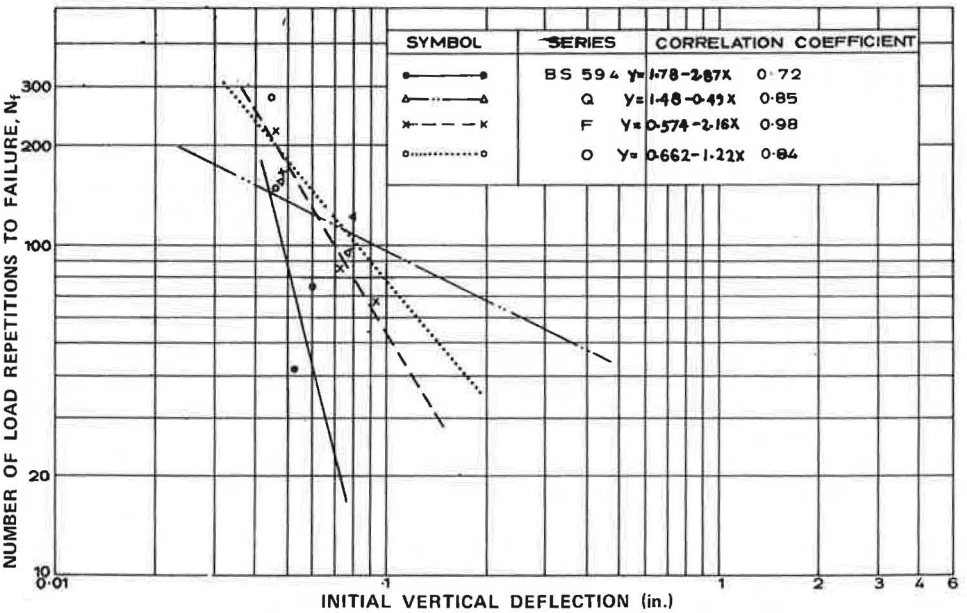

It is apparent from these figures that, whereas the B. S. 594 mix retained its order of merit in both cases, the three dense mixes changed their orders of merit from one figure to another. This was most probably because the initial vertical deflection and increase in vertical deflection are not influenced by the mix properties in exactly the same way.

Mix F, for instance, shows less interlocking than mix q or mix O. Under the action of the load, mix F would suffer more deflection and compaction during the first 50 cycles than the other two mixes. Afterward, the increase in vertical deflection was found to be the lowest (at the OBC) because of the effect of the beam action of the flaky particles and the larger surface area, which would inevitably increase the adhesion.

The orders of merit and OBCs of the four mixes interchanged according to the property analyzed or presented. This means that there is no one unique OBC that gives the maximum fatigue life (Figure 2), minimum initial vertical deflection (Figure 3), and minimum rate of increase in vertical deflection (Figure 4). In the design of a mix, therefore, the binder content should comprise all these properties as well as other requirements such as skid resistance and Marshall stability.

EFFECT OF INITIAL VERTICAL DEFLECTION ON LIFE

Figure 5 shows number of load applications to failure plotted against the corresponding initial vertical deflections (at the 50th cycle of the 3-cm/min rate of deformation) for the four mixes at all binder contents. There is a linear increase in life with the decrease in the initial vertical deflection for each mix; significant correlation coefficients 0.84, 0.94, 0.85, and 0.72 were obtained for mixes O, F, q, and B. S. 594 respectively. No correlation was observed when the results of either the three dense mixes or all four mixes were pooled together.

It is reasonable to infer, however, that the initial vertical deflection could be used to roughly predict the fatigue life of the mix without carrying out the test to failure.

EFFECT OF THE INCREASE IN VERTICAL DEFLECTION ON LIFE

The number of cycles to failure is shown plotted against the corresponding rate of increase in vertical deflection in Figure 6. Linear relationships were obtained with correlation coefficients of 0.87, 0.91, 0.82, and 0.89 for mixes O, F, q, and B. S. 594 respectively. Pooling the results of mixes O, F, and q slightly reduced the correlation to 0.81. When the results of the four mixes were pooled, however, a low (but more significant because of the larger number of results) correlation coefficient of 0.62 was obtained.

This indicates that the increase in vertical deflection bears more relation to the fatigue life than the initial vertical deflection itself. Consequently, this increase in deflection could be used to roughly predict the fatigue life of the mix and to compare mixes without fatigue testing to failure.

In a multiple linear regression analysis, however, life correlated very well with both the initial deflection and the increase in deflection combined. Correlation coefficients of 0.9, 0.996, 0.9, and 0.995 were obtained for mixes O, F, q, and B. S. 594.

Pooling the results of mixes O, F, and q in a similar analysis produced a correlation of 0.84, and it was 0.63 when all four mixes were pooled.

This confirms the view that the three-variable model is superior to the two-variable model as an estimating equation. It also suggests that the combination of initial deflection and the increase in deflection could be used to predict the life better than either of the two variables individually.

Figure 6. Number of load applications to failure versus rate of increase in vertical deflection.

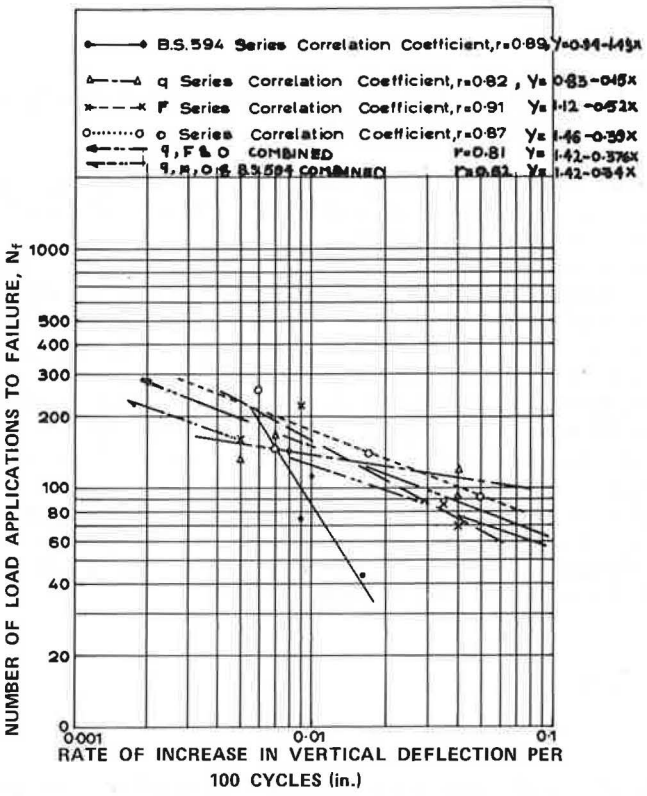

Figure 7. Vertical deflection versus binder content.

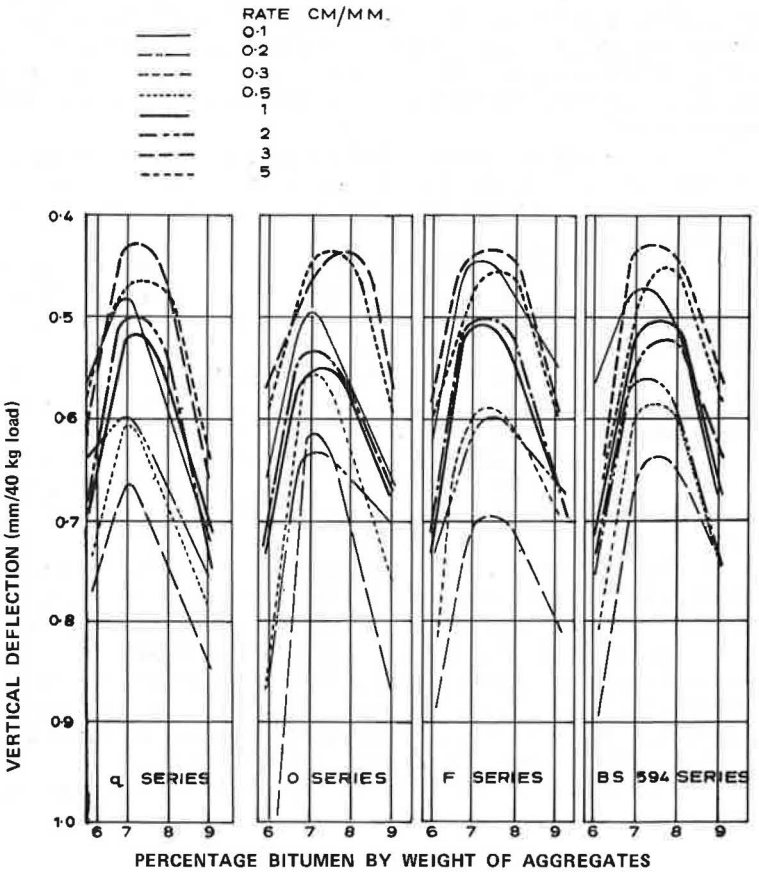

SLAB DEFLECTION VERSUS BINDER CONTENT AT DIFFERENT RATES OF MACHINE DEFORMATION

As mentioned earlier, each slab was first subjected to eight cycles (70-kg load) at 5, 3, 2, 1, 0.5, 0.3, 0.2, and 0.1 rates of deformation, after which the load was applied repeatedly at 3 cm/min until failure.

Slab deflections at each rate versus the corresponding binder content are shown in Figure 7. Minimum values of slab deflection at different OBCs are shown for each rate. The OBC shifted to the dry side as the rate was decreased. An average total decrease in OBC between the two extremes of rates was 0.4, 0.5, 0.4, and 0.3 percent for mixes F, O, q, and B. S. 594 respectively.

It is suggested that high rates of deformation would not give the binder as much time to flow and be mobilized as would low rates. Consequently, more binder was needed at high rates than would be needed at low rates to produce the minimum slab deflection, and this was observed in the OBC shift.

High rates produced sharper curves than low rates, suggesting that the former would be more appropriately used in comparing mixes at different binder contents. Lower rates, on the other hand, appear to be more suitable to investigation of the behavior of the mixes at one binder content than the OBC.

CONCLUSIONS

The results can be summarized as follows.

1. The failure in a slab tested under a repeated load of constant magnitude was defined as the number of cycles at which both the elastic and cumulative permanent deformation curves drawn on a semilog scale deviate from the straight line.
2. A peak value of fatigue life was obtained for each of the four mixes, O, F, q, and B. S. 594, at OBCs of 7.2, 7.2, 7.5, and 7.7 percent by weight of aggregate. The maximum fatigue life at the OBC was exhibited by mix O followed by mixes F, B. S. 594, and q, which suggests that it is beneficial to use a limited amount of flaky particles in the mix. Results also revealed the inferiority of the B. S. 594 mix to the two dense mixes O and F.
3. A minimum value of initial vertical deflection (70-kg load and 3-cm/min rate of deformation) was obtained for each mix; the lowest minimum initial deflection was exhibited by mix q followed by mixes O, F, and B. S. 594 at 7.3, 7.5, 7.4, and 7.5 percent OBCs respectively.
4. For each mix a minimum value of rate of increase in vertical deflection (increase in deflection at 70-kg load and 3-cm/min rate of deformation) was observed, the lowest of which was exhibited by mix F followed by mixes q, O, and B. S. 594 at 7.6, 7.2, 7.3, and 7.7 percent OBCs respectively.
5. There is no one unique OBC that gives the maximum density, maximum fatigue life, minimum initial vertical deflection, and minimum rate of increase in deflection. In the design of a mix, the binder content should comprise all these requirements as well as other properties such as skid resistance and Marshall stability.
6. In a simple linear regression analysis, initial vertical deflection and rate of increase in vertical deflection (increase in deflection) correlated very well with the fatigue life.
7. Mix life could roughly be predicted from either initial deflection or increase in vertical deflection. Increase in deflection can also be used to predict the life of a group of mixes and to compare these mixes without fatigue testing to failure.
8. In a multiple linear regression, life correlated very well with both initial deflection and increase in deflection combined. Correlation coefficients obtained were higher than the corresponding coefficients obtained in a simple regression analysis, indicating that the combination of initial vertical deflection and increase in deflection predicted life better than either of the variables individually.
9. The three rationally designed mixes were generally superior with regard to

fatigue strength to the B. S. 594 wearing course mix made of the same type of stone.

REFERENCES

1. W. J. Kari, C. S. Hughes, and R. V. LeClerc. Compaction of Asphalt Concrete. Symposium, Proc., AAPT, Vol. 36, 1967.
2. P. S. Pell. Fatigue Characteristics of Bitumen and Bituminous Mixes. First International Conference on Design of Asphalt Pavements, Ann Arbor, Mich., 1962.
3. J. A. Deacon. Fatigue of Asphalt Concrete. Univ. of California, PhD thesis, 1965.
4. F. Moavenzadeh and R. A. Carnaghi. Viscoelastic Response of Sand-Asphalt Beams on Elastic Foundations Under Repeated Loading. Proc., AAPT, Vol. 35, 1966.
5. J. A. Deacon and C. L. Monismith. Laboratory Flexural-Fatigue Testing on Asphalt-Concrete With Emphasis on Compound-Loading Tests. Highway Research Record 158, 1967.
6. R. A. Jimenez and R. M. Galloway. Behavior of Asphalt Concrete Diaphragms to Repetitive Loading. Proc., First International Conference on Design of Asphalt Pavements, Ann Arbor, Mich., 1962.
7. J. M. Kirk. Results of Fatigue Tests on Different Types of Bituminous Mixtures. Second International Conference on Design of Asphalt Pavements, Ann Arbor, Mich., 1967.
8. J. A. Epps and C. L. Monismith. Influence of Mixture Variables on the Flexural Fatigue Properties of Asphalt Concrete. Proc., AAPT, Vol. 38, 1969.
9. P. Bazin and J. B. Saunier. Deformability, Fatigue and Healing Properties of Asphalt Mixes. Second International Conference on Design of Asphalt Pavements, Ann Arbor, Mich., 1967.
10. R. Baker and H. Papazian. The Effect of Stiffness Ratio on Pavement Stress Analysis. HRB Proc., Vol. 39, 1960.
11. K. E. Secor and C. L. Monismith. Viscoelastic Response of Asphaltic Paving Slabs Under Creep Loading. Highway Research Record 67, 1965.
12. C. L. Monismith, R. L. Alexander, and K. E. Secor. Rheologic Behavior of Asphaltic Concrete. Proc., AAPT, Vol. 35, 1966.
13. J. P. Nielsen and R. J. Lowe. Design of Parameter for a Layered Pavement System. Proc., AAPT, Vol. 34, 1965.
14. H. M. Westergaard. Stresses in Concrete Pavements Computed by Theoretical Analysis. Public Roads, Vol. 7, No. 1, 1926.
15. D. M. Burmister. The Theory of Stresses and Displacements in Layered Systems. HRB Proc., Vol. 23, 1943.
16. G. Lees. The Rational Design of Aggregate for Dense Composition. Presented at Annual Meeting of AAPT, Feb. 1970.
17. L. E. Wood and W. H. Goetz. Strength of Bituminous Mixtures and Their Behavior Under Reported Loads. HRB Proc., Vol. 36, 1957.

RECOMMENDED PROCEDURE FOR DETERMINING THE DYNAMIC MODULUS OF ASPHALT MIXTURES

Larry L. Yeager, Martin Marietta Cement, Baltimore; and
Leonard E. Wood, School of Civil Engineering, Purdue University

The fundamental properties of asphaltic concrete are important to researchers as input to new design procedures. The dynamic modulus of bituminous mixtures is a rational part of this new design procedure as a predictor of in-service pavement performance. Much research is under way to determine the fundamental properties of bituminous paving mixtures under a wide variety of conditions. The objective of this study was to select a method for evaluating the dynamic modulus of an Indiana state highway surface mixture. The main variables used in this study were stress level, cyclic loading rate, temperature, and asphalt type. A final procedure was developed that incorporates these variables. Material and sample preparation included a study on compaction procedures of 4 by 8-in.-high (102 by 203-mm) cylindrical specimens. A compaction technique was developed that yields uniform bulk density of the specimen. Another objective of the study was to correlate a physical property of the asphalt cement to the dynamic modulus. Such a correlation was established between the dynamic modulus and the slope of log kinematic viscosity versus 1/temperature, the cyclic loading rate, and temperature. This correlation may not be valid for mixtures of different aggregate types, gradation, and asphalt contents.

•EVALUATION of the fundamental relationship between stress and strain of an asphaltic paving mixture has been of great interest to many researchers (1). A form of the relationship known as the complex modulus has been studied extensively. The complex modulus is a complex number that defines the relationship between stress and strain for a linear viscoelastic material subjected to a sinusoidal loading.

When a linear viscoelastic material is subjected to a loading stress of the form $\sigma = \sigma_o \sin (wt)$, the resulting strain is $\epsilon = \epsilon_o \sin (wt - \phi)$, which lags the stress by the phase angle ϕ. The complex modulus E* is defined as

$$E^* = E' + jE'' \tag{1}$$

where

E^* = complex modulus,

$E' = \frac{\sigma_o}{\epsilon_o} \cos \phi$,

$E'' = \frac{\sigma_o}{\epsilon_o} \sin \phi$,

j = imaginary number,

σ_o = maximum stress applied in psi (kPa),

Publication of this paper sponsored by Committee on Characteristics of Bituminous Paving Mixtures to Meet Structural Requirements.

ϵ_o = maximum strain experienced during test in in./in. (mm/mm), and
ϕ = phase lag angle in deg.

Based on this definition, the absolute value of the complex modulus $|E^*|$ is a measure of the material's elasticity and ϕ is a measure of the viscous response.

The absolute value of the complex modulus is commonly referred to as the dynamic modulus and is defined as

$$|E^*| = \frac{\sigma_o}{\epsilon_o} \quad (2)$$

The procedure for determining the dynamic modulus and the results obtained from those tests are the main concern of this research.

Current literature (1) provides ample background on isolating those factors that influence the dynamic modulus; however, the concept of correlating a physical property of the asphalt cement to the dynamic modulus is still not prevalent in the literature.

The primary objective of this study was to evaluate and select a procedure for determining the dynamic modulus of surface mixtures used by the Indiana State Highway Commission (ISHC).

Currently, special equipment is needed to adequately evaluate dynamic modulus. If a correlation between the physical characteristics of the asphalt cement and the dynamic modulus of the asphaltic paving mixture is established, a different approach to design might ensue.

Thus a secondary objective of this project was to quantify physical and rheological properties of asphalt cement to establish a correlation between an asphalt property and the dynamic modulus of the mixture.

AGGREGATES

Sources and Types

The aggregates in this study were 100 percent crushed limestone obtained from the Pipe Creek Stone Company of Sweetser, Indiana. This producer is listed as quarry 162 by the Indiana State Highway Commission (2, 3).

The geologic setting for this material is the Liston Creek limestone member (Huntington litheface) of the Wabash formation of the Silurian period (4). A typical section of this formation contains a bluish gray to tan limestone that is cherty, fine grained, slightly fossiliferous, and usually thin bedded. Generally, the Liston Creek member is tough and can pass soundness and abrasion tests, but it contains abundant chert with a specific gravity less than 2.45 (5, 6).

Preparation

Material for this study originated from the far north of the quarry and received the normal commercial crushing and sizing. ISHC gradation sizes 8 and 53 were obtained from the producer's stockpiles and transported to the Purdue Bituminous Materials Laboratories where they were resized to logarithmic sieve fractions and washed.

Specification Tests and Physical Properties

Unless otherwise stated or required by standard methods, all tests were performed on each of the fractions. The gradation chosen for this study meets the requirements

of ISHC surface mixture 9A and mixture IVb of the Asphalt Institute (7). The sieve analysis is as follows:

Sieve Size	Percentage Passing
¾ in.	100
½ in.	82
⅜ in.	70
No. 4	51
No. 8	40
No. 16	30
No. 30	20
No. 50	12
No. 100	7
No. 200	3

ASPHALT

Three penetration grades of asphalt were used: 60/70 for hard asphalt, 85/100 for normal asphalt, and 120/130 for soft asphalt.

A set of standard acceptance tests was run on each of the asphalts to characterize them. Results of these tests are given in Table 1. The asphalt was produced by the American Oil Company. Figure 1 shows the relationship between kinematic viscosity and temperature for this asphalt.

MIX DESIGN

The centrifuge kerosene equivalent method described in Asphalt Institute Manual Series 2 was used to estimate asphalt content for each of the three asphalt types.

ASTM Designation D 1560 and Designation D 1561 were used to finalize the asphalt contents for the bituminous paving mixtures included in this study. Design asphalt contents for the dense-graded bituminous surface paving mixture were as follows:

Asphalt	Asphalt Content (percent)
Hard, type 101	6.7
Medium, type 102	6.5
Soft, type 103	6.3

All asphalt contents are based on weight of dried aggregate.

COMPACTION METHODS

Specimens for this study were prepared according to ASTM Designation D 1561 except that the compacted height of the specimen, specific foot pressure, and number of tamping blows were modified.

Numerous variations of ASTM D 1561 were tried so that the best method of compaction yielding the greatest uniformity could be used. Consideration was given to foot pressure and number of blows needed to compact an 8-in. (203-mm) specimen yet still follow as closely as possible ASTM method D 1561. A summary of methods and results

of these various methods follows.

1. Method A—ASTM D 1561 was used for this method except that an 8-in.-high (203-mm) specimen rather than a 2½-in. (64-mm) specimen was compacted. The mixture was heated to 230 F (110 C), placed in a filling trough, fed into the mold, and rodded. Half of the material was placed into the mold and rodded 40 times (20 around the edge and 20 in the center). The other half was then added and rodded in the prescribed manner. A leveling type of kneeding compaction at 250-psi (1720-kPa) foot pressure was applied for 30 tamps at which time the foot pressure was increased to 500 psi (3445 kPa) and applied for 150 tamps (5 minutes).
2. Method B—ASTM D 1561 was followed except for specimen height and addition of mixture to the mold. Four 2-in. (50-mm) layers were used instead of the ordinary two layers. One-quarter of the mix was placed in the filling trough and then loaded into the mold. Each layer was rodded 40 times (20 around the edge and 20 in the center) and then tamped 4 to 10 times at a foot pressure of 250 psi (1720 kPa). Once the top layer was compacted at 250 psi, 500 psi (3445 kPa) was applied for 150 tamping blows.
3. Method C—ASTM D 1561 was followed except that specimen height, specific foot pressure, and number of tamping blows were varied. The mixture was placed in the filling trough and added continuously to the mold. The tamping foot compacted the mixture at 250-psi (1720-kPa) foot pressure throughout the filling process. This method of compaction causes the tamping foot to raise as more material is added, thus forcing the foot to walk out of the specimen mold. The entire process takes 2 min or 60 tamping blows. After 60 blows, the foot pressure was increased to 500 psi (3445 kPa) and was continued for 150 tamping blows. There was no rodding of the material in this method.
4. Method D—All of the material was introduced into the mold at one time and rodded 20 times around the edge and 20 times in the center. A compactive effort of 500 psi was placed on the specimen for a total of 200 tamping blows.
5. Method E—The effectiveness of the double plunger method of compaction was also studied. All of the material was placed into the mold and the double plunger method was used to compact the specimen. The load was placed on the specimen at the rate of 0.05 in./min (1.27 mm/min) to an ultimate load of 1,000 psi (6.9 MPa).

In all five methods, the mixture was heated to 230 F (110 C) before it was compacted. A 1,000-psi (6.9-MPa) double plunger static load was applied at the rate of 0.05 in./min (1.27 mm/min), after the kneading compaction was completed and the specimen cooled in a 140 F (60 C) oven for 1½ hours.

After cooling, the specimens were weighed in air and water, and the bulk specific gravities were calculated. The specimens were then cut into eight 1-in. (25-mm) slices with a diamond-edged masonry saw. Bulk specific gravities of the slices were determined. The complete analysis of compaction technique and selection of the method to be used in this study is given in Table 2.

The standard deviations for the compaction methods used were calculated from

$$S.D. = \left[\frac{1}{N-1}(X_1 - \overline{X})^2\right]^{1/2} \quad (3)$$

where

N = number of slices,
X_1 = density of each slice, and
$\overline{X}$ = average density of N slices.

The percentage of variation was calculated as

Table 1. Results of asphalt cement characterization tests.

Specification	Asphalt Designation 101	102	103
Penetration at 25 C, 100 g, 5 sec	56	85	122
Ductility at 25 C, 5 cm/min	100+	100+	100+
Specific gravity at 25 C	1.028	1.027	1.022
Thin film oven test at 163 C for 5 hours, percentage of original penetration	58.2	66.0	66.7
Solubility in CCl_4, percent	99.6	99.7	99.7
Viscosity			
Absolute at 60 C, poises	2,213	1,236	678
Kinematic at 135 C, stokes	3.68	3.05	2.29
Softening point, F	129.2	121.3	113.3
Penetration index	+0.03	+0.06	-0.008

Note: 1 poise = 0.1 Pa·s; 1 stoke = 0.0001 m^2/s; 1 F = 1.8 C + 32.

Figure 1. Kinematic viscosity versus temperature.

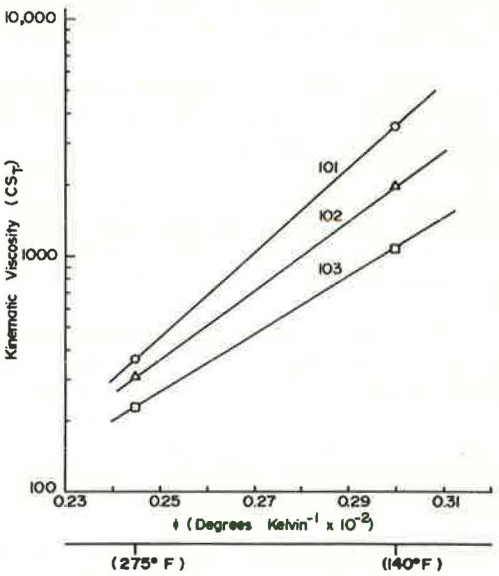

Table 2. Results of compaction study.

Method	Average Absolute Value of the Percentage of Variation	Standard Deviation
A	2.905	4.98
B	2.033	3.78
C	0.988	1.86
D	1.313	2.24
E	2.617	4.81

$$\text{Percentage of variation} = \frac{(\overline{X} - X_i)}{\overline{X}} \times 100 \quad (4)$$

The absolute value of the percentage of variation was added for each of the slices and then divided by the number of slices. This value was termed the average absolute value of the percentage of variation (Table 2).

Method C was chosen as the compaction technique because it gives the best uniform bulk density throughout the specimen and one that closely resembles the bulk density of a compacted Hveem specimen at the design asphalt content using ASTM D 1561. This fact can be seen in comparing the standard deviation and average absolute value of the percentage of variation.

PROCEDURE FOR MEASURING DYNAMIC MODULUS

In the dynamic modulus tests, unconfined cylindrical specimens of a dense-graded bituminous concrete surface mixture were compacted and cured as described. The 4-in.-diameter by 8-in.-high (102 by 203-mm) specimens were subjected to sinusoidal stresses of differing amplitudes, frequencies, and temperatures, and the amplitudes and phase lag angle differences of the resulting axial strains were studied. Loading of the specimens was accomplished with an electric-hydraulic testing system. For the dynamic modulus tests, the sinusoidal loads were applied with the testing systems hydraulic actuator through hardened steel platform loading disks placed at either end of the specimen. A sulfur-based cement compound was used to cap the cylindrical specimens to ensure parallel planes of loading. A Baldwin-Hamilton type T2G1 50,000-lb capacity (222 400-N) load cell was used to measure the loads applied. Strain was measured according to two independent methods. Baldwin-Lima-Hamilton SR4 type A-1 strain gauges were cemented vertically to the specimen at the midpoint of the 8-in. (203-mm) length with Bean BR 104 epoxy adhesive in accordance with manufacturer's recommended procedure.

Temperature compensation gauges were incorporated into the circuit. The output from the half-bridge strain gauge setup was recorded by a dual-channel recorder. Duplicate strain gauge setups were prepared on opposite sides (180 deg apart) of each of the specimens, and the output from each gauge set was recorded simultaneously. An average value was determined from the duplicate gauge to calculate the strain response.

Strain was also measured by a linear variable differential transformer (LVDT) built into the actuator of the electric-hydraulic testing machine. The outputs from the LVDT and from the load cell were recorded on a two-channel recorder.

Specimens were brought to test temperature by means of a walk-in freezer for 40 F (4.4 C) specimens and a forced-air oven for 70 and 100 F (21 and 38 C) specimens. Care was taken to ensure the fastest possible testing of the specimen so that only a minimum change in temperature would occur. The temperature in the laboratory was held at a constant temperature of 70 F (21 C).

To determine the temperature change that might result from testing the specimens at temperatures other than 70 F (21 C), a study of temperature change versus time was made. An $\frac{1}{8}$-in. (3.2-mm) hole was drilled to the center of a 4 by 8-in.-high (102 by 203-mm) specimen at midheight. A temperature probe was placed in the hole, and the specimen was brought to the test temperature. An average of six tests gave the result that it take 12 min to change the temperature 1 deg F. The testing of the specimen lasted from 2 to 7 min.

The stress levels were 50 and 100 psi (345 and 689 kPa); loading frequencies were 1, 6, and 12 cps; the tests were run at 40, 70, and 100 F (4.4, 21, and 38 C); and the three asphalt cements were 56, 85, and 122 penetration. The aggregate gradation was the same for all tests.

Two additional tests were made for comparison. Three specimens were soaked for 4 days at 122 F (50 C) to determine qualitatively the effect of soaking on the dynamic modulus value.

A set of specimens instrumented with strain gauges was tested to compare strain gauge and LVDT results. Consistent data were obtained for both types of strain measurement, indicating that either method is equally adequate for measuring strain at the stress level used in this investigation. The stress-strain relationship was calculated at the point in time when the amplitude of the steady-state recoverable axial strain in sinusoidal loadings becomes constant. This usually was between 100 to 300 cycles.

Results of the Dynamic Modulus Test

The primary objective of this study was to evaluate and select a procedure for determining the dynamic modulus of ISHC surface mixtures. The results of the modulus tests are given in Table 3.

Dynamic modulus measurements were made on one or two specimens at each indicated stress level, temperature, loading rate, and asphalt type. Tests of only one specimen were replicate tests performed by using the procedure of Kallas and Riley (9).

The phase lag angle is not used in the dynamic modulus calculation, but is useful in the calculation of the complex modulus. The phase lag angles were calculated from the tests used for quantitative comparison. These ϕ values are also given in Table 3.

Table 4 gives the data taken in two special test conditions. The first set of data was calculated from results of tests using SR-4 strain gauges instead of the LVDT to measure specimen deformations. In the strain gauge measurements, ϕ was not recorded.

The second set of data was recorded for tests performed on soaked specimens. Each of the three specimens was placed in a water bath for 4 days and held at a constant temperature of 122 F (50 C). The other variables remained the same. For comparison purposes, the reader is directed to examine Tables 3 and 4 for the similar circumstances concerning the test conditions.

Test data (Figures 2 through 7) show the relationship of the $\log_{10}\log_{10}$ (dynamic modulus) versus $\log_{10}$ (loading frequency). Each graph is plotted at one load stress level and for one asphalt type. The three lines represent the relationship between $\log_{10}\log_{10}$ (dynamic modulus) and $\log_{10}$ (frequency) at 1, 6, and 12 cps for temperatures of 40, 70, and 100 F (4.4, 21, and 38 C).

Influence of Variables on the Dynamic Modulus

The values of the dynamic modulus may be influenced by a number of variables. The four controlled variables were temperature, frequency, stress level, and asphalt type.

Temperature

$|E^*|$ and ϕ are a function of the temperature at which the test is performed. Figures 2 through 7 show that, for a given set of conditions, the dynamic modulus value decreases with an increase in temperature. For a stress level of 50 psi (345 kPa) and a loading rate of 1 cycle/sec (Figure 2), the modulus decreases from 200 ksi (1380 MPa) at 40 F (4.4 C) to 40.9 ksi (282 MPa) at 100 F (38 C). Similar results may be seen at other stress levels, cyclic loading rates, and asphalt types. At 12 cycles/sec and a load stress level of 50 psi (345 kPa), the value of the dynamic modulus varied from 1,141 ksi (7860 MPa) for 40 F (4.4 C) to 800 ksi (5520 MPa) for 100 F (38 C).

In all cases, the trend of a higher dynamic modulus at a lower temperature was not unexpected because of the viscoelastic character of the bituminous paving mixture.

Table 3. Values of dynamic modulus and phase angle.

Group	Load (psi)	Temperature (F)	|E*| (ksi) 1 cps	|E*| (ksi) 6 cps	|E*| (ksi) 12 cps	ϕ (deg) 1 cps	ϕ (deg) 6 cps	ϕ (deg) 12 cps
601	50	40	200.0	571.4	1,144.1	10.8	7.2	3.4
		70	133.3	546.5	888.0	13.5	10.4	6.8
			131.0	540.5				
		100	40.9	333.3	800.0	19.8	15.3	10.4
	100	40	320.4	680.2	1,066.6	16.4	14.3	12.6
				552.4				
		70	226.5	591.7	888.0	21.6	20.1	15.7
				591.7				
		100	125.0	450.0	759.6	26.6	21.4	21.0
602	50	40	330.0	864.9	1,068.4	18.0	8.6	5.6
		70	246.5	592.4	888.0	23.4	13.8	9.3
			242.5	551.8				
		100	29.7	333.0	728.0	28.8	19.3	13.8
	100	40	410.5	666.6	1,066.6	19.4	15.5	13.4
				653.5				
		70	268.0	561.7	888.0	26.3	20.8	17.8
				552.4				
		100	90.3	430.6	795.8	28.1	25.3	24.0
603	50	40	340.0	800.0	915.8	19.4	12.4	7.2
		70	320.5	553.9	888.0	26.9	20.1	15.3
			265.0					
		100	30.6	325.0	800.0	30.4	27.8	19.6
		40	456.7	666.6	1,066.6	23.9	20.1	15.7
				641.0				
		70	232.0	531.9	888.0	29.8	28.4	21.6
				531.9				
		100	100.4	445.9	800.0	36.5	34.3	33.0

Note: 1 psi = 6.9 kPa; 1 F = 1.8 C + 32; 1 ksi = 6.9 MPa.

Table 4. Dynamic moduli of special tests.

Group	Load (psi)	Temperature (F)	Frequency (cps)	|E*| (ksi) SR-4	|E*| (ksi) LVDT	|E*| (ksi) Soaked[a]	|E*| (ksi) Dry
601	50	70	1	164.5	132	40.0	132
602	50	70	1	208.3	245	40.0	245
603	50	70	1	333.3	293	34.9	293

Note: 1 psi = 6.9 kPa; 1 F = 1.8 C + 32.

[a]Specimens were soaked for 4 days at 122 F (50 C).

Figure 2. Log_{10} log_{10} dynamic modulus versus log_{10} frequency (type 101 asphalt, 50-psi stress).

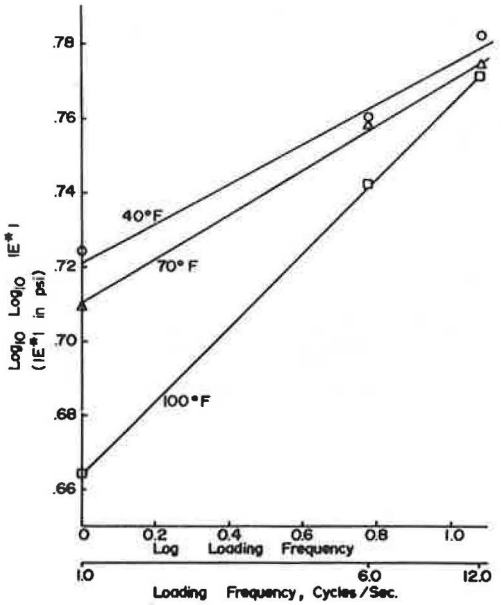

Figure 3. Log_{10} log_{10} dynamic modulus versus log_{10} frequency (type 102 asphalt, 50-psi stress).

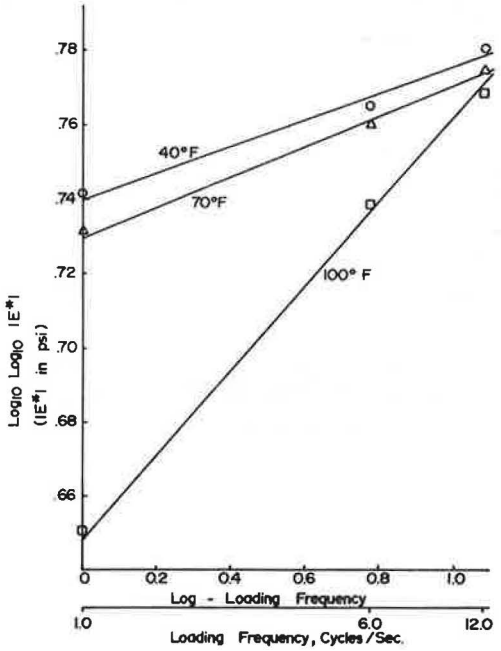

Figure 4. Log_{10} log_{10} dynamic modulus versus log_{10} frequency (type 103 asphalt, 50-psi stress).

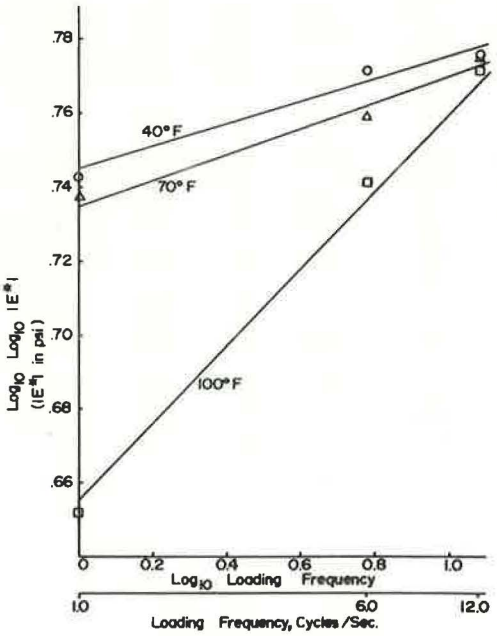

Figure 5. Log_{10} log_{10} dynamic modulus versus log_{10} frequency (type 101 asphalt, 100-psi stress).

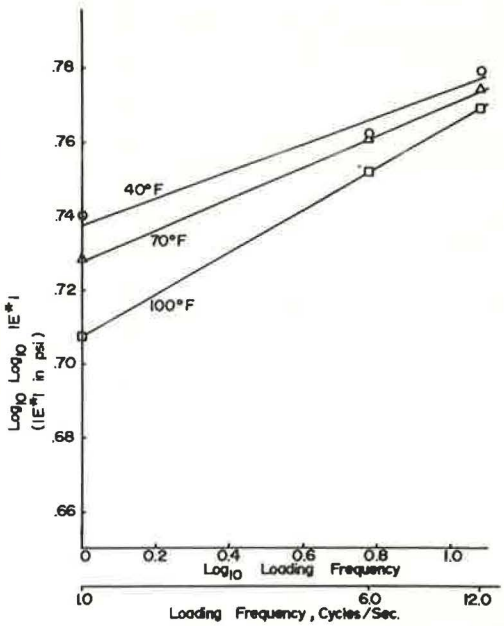

Figure 6. Log_{10} log_{10} dynamic modulus versus log_{10} frequency (type 102 asphalt, 100-psi stress).

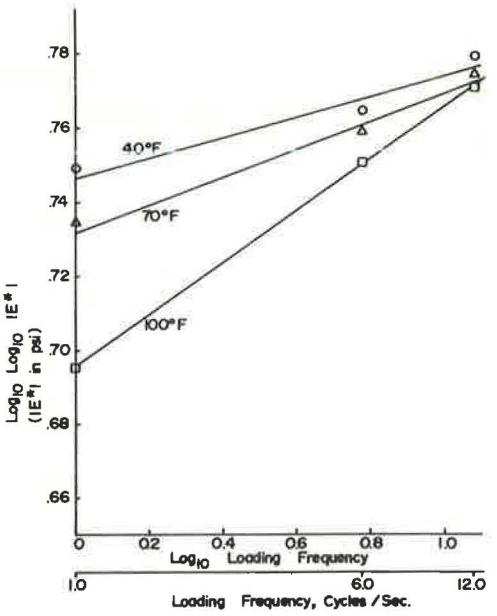

Figure 7. Log_{10} log_{10} dynamic modulus versus log_{10} frequency (type 103 asphalt, 100-psi stress).

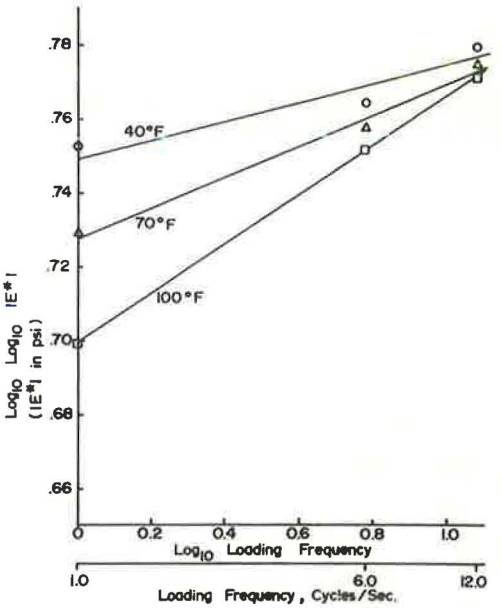

Frequency

The variation of the dynamic modulus value with the frequency of load application is a basic property of an asphaltic concrete mixture. The response of a viscoelastic mixture directly depends on the time of loading and the temperature at which the test is made. Similar results of the dynamic modulus value may be obtained at two different temperatures by simply changing the rate of loading at one of the temperatures. This is known as the time-temperature superposition principle (10). The frequency of load application has a direct effect on the response.

A rapid frequency of loading (e.g., 12 cps) does not allow the specimen enough time to flow, and thus the specimen acts more elastically. Slower rates of loading (e.g., 1 cps) allow the specimens to flow, which, in turn, yields a larger total strain. The modulus value becomes less at the slower rates of loading because of the larger total strain.

For a stress level of 50 psi (345 kPa), a temperature of 40 F (4.4 C), and asphalt type 101, the modulus value increases from 200 to 1,144 ksi (138 to 7880 MPa) as the rate of loading increases from 1 to 12 cps.

All asphalt types, stress levels, and temperatures resulted in an increase in dynamic modulus value with an increase in cyclic rate. That the dynamic modulus increased as the frequency of loading increased was not unexpected because of the viscoelastic character of the bituminous paving mixture.

The importance of frequency has already been established. The range of frequencies used in this study can be related to studies that correlate vehicle speed to frequency of load application. Coffman (11) concluded that a vehicle acts as a cyclic load with a wavelength of 6 ft (1.8 m). Therefore, vehicle speed can be related to test frequencies by

$$V = \lambda f \tag{5}$$

where

V = velocity in ft/sec (m/s),
f = frequency in sec^{-1}, and
λ = wavelength of a car in ft (m).

Based on this relationship, the loading frequencies of 1, 6, and 12 cps used in this study represented speeds of 0.5, 25, and 50 mph (0.8, 40, and 80 km/h) respectively.

Stress Level

By definition, a linear material is one whose stress-strain ratio (a modulus value) is independent of the level of stress applied. It is commonly accepted that an asphaltic concrete mixture is not a linear material. However, it is possible to characterize an asphaltic concrete mixture at low stress levels when its behavior approximates that of a linear material. Stress levels of 50 and 100 psi (345 and 690 kPa) were chosen to approximate tire pressures experienced by the pavement in service. It is accepted by many researchers that linear results of the dynamic modulus test may be obtained in total compression tests up to a maximum value of 70 psi (480 kPa) for temperatures of 40, 70, and 100 F (4.4, 21, and 38 C). It can be seen in Table 3 that, for temperatures, asphalt contents, and cyclic loading rates, the dynamic modulus values are similar at 50 and 100 psi (345 and 690 kPa) except at a cyclic stress of 100 psi (690 kPa) at the extreme conditions of 100 F (38 C) temperature and 1-cps loading rate.

Asphalt Type

The assumption is that the higher penetration asphalts used in asphaltic concrete mixtures tend to lower the dynamic modulus, all other factors remaining the same. However, the significance of asphalt type on dynamic modulus values was minimal in this study.

Correlation Between Dynamic Modulus and an Asphalt Property

A secondary objective of this study was to establish a correlation between the dynamic modulus and some physical property of the asphalt cement. The slope of the log kinematic viscosity versus 1/temperature curve for the asphalt cements was chosen as the index to quantify the various binders. The temperature at which the dynamic modulus test was conducted and the frequency of loading were other variables incorporated into the correlation equation. The form of the equation is

$$\text{Log } |E^*| = \log (x_1)(x_2) + x_3 \qquad (6)$$

where

x_1 = slope of log kinematic viscosity versus 1/T curve,
$x_2 = \log T - \left(\frac{\log T - \log 40}{0.710} \right)$,
x_3 = log frequency of loading in cps, and
T = test temperature in F (C).

These variables were selected because they affected the dynamic modulus more significantly in this study than any of the other variables. The variables represent a viscous character, a temperature, and a loading rate.

Table 5 gives the logarithms of the dynamic moduli from the experimental tests and from equation 6. The comparison in Table 5 is for asphalt type 101, tested at a stress level of 50 psi (345 kPa). A comparison of the experimental and calculated values of the $\log_{10} |E^*|$ versus the $\log_{10}$ loading frequency is shown in Figure 8. Closest correlation may be seen for these data at 1, 6, and 12 cps at 100 F (38 C).

Effect of Moisture on Dynamic Modulus

The effect of moisture due to field exposure on the dynamic modulus of bituminous mixtures could be of importance to the flexible pavement designer. It was the intent of this study to determine the effect of moisture on dynamic modulus values. The mixtures were moistened by soaking the specimens for 4 days in a water bath at 122 F (50 C). The dynamic modulus values at 70 F (21 C), 50 psi (345 kPa), and 1 cps are considerably less for the soaked specimens than for the unsoaked specimens (Tables 3 and 4). This reduction is probably a function of the aggregate type as well as gradation and asphalt content and type. However, reducing the dynamic modulus value of a soaked specimen is significant and could be of great importance to the flexible pavement designer if it could be correlated to field exposure.

A RECOMMENDED PROCEDURE FOR DETERMINING THE DYNAMIC MODULUS OF ISHC SURFACE MIXTURES

A testing device capable of measuring small strains and recording load and deformation simultaneously is essential to determining the dynamic modulus of an asphaltic

Table 5. Calculated and experimental values (in ksi) of dynamic modulus.

Temperature (F)	cps	Experimental	Calculated
40	1	5.301	5.206
	6	5.757	5.945
	12	6.058	6.285
70	1	5.120	4.884
	6	5.735	5.662
	12	5.948	5.963
100	1	4.612	4.680
	6	5.522	5.458
	12	5.903	5.759

Note: 1 F = 1.8 C + 32.

Figure 8. Calculated and experimental values of dynamic modulus versus cyclic loading rate.

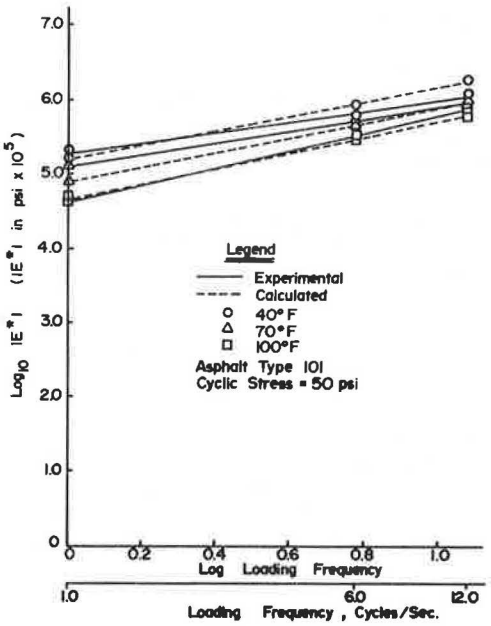

concrete mixture. An electro-hydraulic testing machine with a dual-channel recorder is widely used in the area of dynamic modulus measurements.

A compaction technique for 4 by 8-in. (102 by 203-mm) specimens that yields uniform bulk density throughout the specimen is very important in the dynamic modulus measurement test and is recommended for compaction of specimens of ISHC surface mixtures. The technique follows ASTM D 1561 except for specimen height, specific foot pressure, and number of tamping blows. The mixture is placed into the filling trough and added continuously to the mold. The tamping foot compacts the mixture at 250 psi (1720 kPa) foot pressure throughout the filling process. This causes the tamping foot to raise as more material is added, thus forcing the foot to walk out of the specimen mold. This process takes 2 min or 60 tamping blows. Then the foot pressure is increased to 500 psi (3445 kPa) and continued for 5 min or 150 tamping blows. The material is not rodded. The molded specimen is then placed in a 140 F (60 C) oven for 1½ hours at which time a 1,000-psi (6.9-MPa) double plunger static load is applied at the rate of 0.05 in./min (1.3 mm/min).

The number of specimens needed to evaluate the dynamic modulus depends on the number of variables being considered. There should be one specimen for each combination of variables. These specimens may be tested twice at the same conditions to replicate the results.

Inasmuch as the relationship between dynamic modulus and a reasonable stress level is linear, a single stress level of 50 psi (345 kPa) is recommended. This stress level tends to simulate the pattern of traffic on an asphaltic pavement.

Temperature and rate of loading are the two most important variables of the dynamic modulus test. Therefore, it is recommended that three rates of loading and three temperatures be used in a test program. The three rates of loading recommended are 1, 6, and 12 cps, which is equivalent to speeds of 0.5, 25, and 50 mph (0.8, 40, and 80 km/h) and closely resembles speeds experienced on many bituminous pavements. Temperatures of 40, 70, and 100 F (4.4, 21, and 38 C) are recommended. Although these temperatures do not cover the entire range of temperatures experienced in the

field, they are attainable in laboratory testing.

CONCLUSIONS

This study developed a procedure for determining the dynamic modulus of an ISHC surface mixture. Within the framework of this study, which was limited to a specific aggregate type, gradation, asphalt type, and asphalt content, the following conclusions were drawn:

1. The relationship between the dynamic modulus of an ISHC surface mixture and certain variables (temperature, loading rate, and a function of original asphalt viscosity versus temperature plot) is

$$\text{Log } |E^*| = \log(x_1)(x_2) + x_3 \quad (6)$$

2. Soaking a 4 by 8-in. (102 by 203-mm) specimen for 4 days in a 122 F (50 C) water bath markedly reduced the dynamic modulus value for the particular aggregate type used in this study and minimized the role of the asphalt.
3. A stress level of 100 psi at a temperature of 100 F (38 C) and cyclic rate of 1 cps resulted in nonlinear values of dynamic modulus.

REFERENCES

1. J. R. Shook and B. F. Kallas. Factors Influencing Dynamic Modulus of Asphalt Concrete. Proc., AAPT, Vol. 38, 1969.
2. C. Lockhart. Indiana Aggregate Sources and Bituminous Mixing Plants for State Highway Use. Indiana State Highway Commission, Jan. 1969.
3. Index of Aggregate Producer for Aggregate Source Map. Indiana State Highway Commission, Jan. 1970.
4. C. H. Ault and D. D. Carr. Directory of Crushed Stone, Ground Limestone, Cement and Lime Producers in Indiana. Indiana Geological Survey, 1970.
5. D. D. Carr, R. R. French, and C. H. Ault. Crushed Stone Aggregate Resources of Indiana. Indiana Department of Natural Resources, Geological Survey Bulletin 42-H, 1971.
6. R. D. French. Crushed Stone Resources of the Devonian and Silurian Carbonate Rocks of Indiana. Indiana Department of Natural Resources, Geological Survey Bulletin 37, 1967.
7. Asphalt Handbook. The Asphalt Institute, Manual Series 4, 1970.
8. Bituminous Materials: Soils; Skid Resistance. American Society for Testing and Materials, Part II, 1969.
9. B. F. Kallas and J. C. Riley. Mechanical Properties of Asphalt Pavements Materials. Proc., Second International Conference on Structural Design of Asphalt Pavements, Aug. 1967.
10. T. Alfrey and E. F. Gurnee. Organic Polymers. Prentice-Hall, 1967.
11. B. S. Coffman. Proc., Second International Conference on the Structural Design of Asphalt Pavements, Aug. 1967, p. 819.

TEMPERATURE DISTRIBUTIONS IN ASPHALTIC CONCRETE PAVEMENTS

H. F. Southgate and R. C. Deen, Bureau of Highways,
Kentucky Department of Transportation

The straight-line relationship derived from Maryland data between temperatures at a given depth and the surface temperatures plus 5-day average air temperatures is as valid for upper New York State and Arizona as for Maryland. The main differences were in the annual ranges and annual mean temperatures. The concept for estimating pavement temperature distributions appears to be valid and may be used with confidence for estimating pavement temperatures at all latitudes and longitudes.

•ASPHALTS are susceptible to temperature change. Similarly, the structural responses of bituminous concrete pavement systems to traffic loadings vary with temperature fluctuations. Surface deflection or rebound is a readily measurable response of a pavement system to a load. The correlations between loads and deflections may be improved by adjusting measured deflections to an equivalent deflection at a common (or base) temperature to reduce the effect of the temperature variable. Under normal conditions of measuring surface deflection, only the surface temperature at the time of measurement can be conveniently determined. Previous analyses indicated that the long-term influences on pavement temperature could be reasonably accounted for by using a 5-day air temperature history. Accordingly, a technique (1) for adjusting pavement deflection measurements to a reference mean pavement temperature was developed. Mean pavement temperatures were estimated from the measured pavement surface temperature at the time of the deflection measurement and the mean daily air temperatures for the previous 5 days as an indication of the air temperature history. This method was simplified by the Asphalt Institute (2).

The method of estimating pavement temperatures at depths raised several questions:

1. What is the effect on the accuracy of the temperature estimating system of such variables as altitude, latitude, longitude, and solar exposure?
2. Does the straight-line relationship (1) based on Maryland data (3) hold true for data from other locations?
3. If other data sets are combined with the Maryland data, does the accuracy of the estimate increase?
4. Can graphs developed from the Maryland data set be used with confidence for other locations?

To answer these questions required that additional data sets be acquired and analyzed. Straub (4) of Clarkson College in upper New York and Jimenez (5) of the University of Arizona, Tucson, supplied data sets for this analysis. Their cooperation is greatly appreciated.

Publication of this paper sponsored by Committee on Characteristics of Bituminous Paving Mixtures to Meet Structural Requirements.

Table 1. Temperature distributions in asphaltic concrete pavements at 8:00 a.m.

Depth (in.)	Data Set	A	B	R	S.E.
2	Maryland	-3.6	0.533	0.985	3.0
	New York	-0.5	0.520	0.985	2.8
	Arizona	-1.9	0.525	0.995	2.0
	Combined	-2.2	0.527	0.988	2.9
	Adjusted	-2.3	0.527	0.988	3.0
4	Maryland	-1.4	0.528	0.987	2.8
	New York	0.3	0.523	0.986	2.8
	Arizona	2.3	0.504	0.994	2.0
	Combined	0.0	0.520	0.989	2.7
	Adjusted	0.5	0.516	0.990	2.7
6	Maryland	0.3	0.531	0.988	2.7
	New York	1.0	0.530	0.986	2.8
	Arizona	5.2	0.497	0.994	1.9
	Combined	1.5	0.523	0.990	2.7
	Adjusted	1.7	0.519	0.989	2.7
8	Maryland	1.6	0.535	0.987	2.9
	New York	1.4	0.537	0.986	2.9
	Arizona	7.9	0.494	0.994	2.0
	Combined	2.5	0.529	0.989	2.8
	Adjusted	2.9	0.523	0.990	2.7
10	Maryland	2.7	0.536	0.985	3.1
	New York	2.0	0.540	0.985	2.9
	Arizona	10.5	0.489	0.992	2.2
	Combined	3.4	0.532	0.987	3.0
	Adjusted	3.8	0.526	0.988	2.9
12	Maryland	4.3	0.532	0.983	3.3
	New York	3.8	0.532	0.982	3.2
	Arizona	11.3	0.486	0.992	2.2
	Combined	5.1	0.526	0.985	3.2
	Adjusted	5.5	0.520	0.986	3.1

Note: 1 in. = 25 mm.

Table 2. Temperature distributions in asphaltic concrete pavements at 10:00 a.m.

Depth (in.)	Data Set	A	B	R	S.E.
2	Maryland	-3.5	0.532	0.987	3.1
	New York	-1.1	0.531	0.984	3.3
	Arizona	-6.4	0.540	0.995	2.2
	Combined	-1.8	0.522	0.988	3.3
	Adjusted	-2.1	0.527	0.988	3.3
4	Maryland	-2.2	0.501	0.978	3.8
	New York	1.3	0.489	0.979	3.5
	Arizona	-4.2	0.502	0.991	2.8
	Combined	0.0	0.485	0.982	3.7
	Adjusted	0.2	0.486	0.984	3.6
6	Maryland	-1.0	0.488	0.970	4.3
	New York	3.0	0.467	0.968	4.3
	Arizona	-1.9	0.485	0.988	3.0
	Combined	1.2	0.472	0.977	4.1
	Adjusted	1.2	0.473	0.978	4.1
8	Maryland	0.2	0.484	0.967	4.5
	New York	3.8	0.462	0.962	4.6
	Arizona	0.6	0.474	0.987	3.1
	Combined	2.2	0.468	0.975	4.2
	Adjusted	2.8	0.464	0.976	4.2
10	Maryland	1.4	0.482	0.966	4.6
	New York	4.2	0.465	0.963	4.5
	Arizona	3.1	0.463	0.985	3.2
	Combined	3.5	0.465	0.975	4.3
	Adjusted	3.9	0.463	0.975	4.3
12	Maryland	2.8	0.479	0.965	4.6
	New York	5.8	0.456	0.960	4.7
	Arizona	4.7	0.457	0.986	3.1
	Combined	4.9	0.460	0.974	4.3
	Adjusted	5.4	0.457	0.974	4.3

Note: 1 in. = 25 mm.

Table 3. Temperature distributions in asphaltic concrete pavements at noon.

Depth (in.)	Data Set	A	B	R	S.E.
2	Maryland	-2.5	0.546	0.989	3.2
	New York	-2.4	0.565	0.986	3.8
	Arizona	-7.4	0.563	0.993	2.7
	Combined	-1.4	0.541	0.988	3.8
	Adjusted	-1.7	0.547	0.988	3.7
4	Maryland	0.1	0.482	0.983	3.6
	New York	1.1	0.493	0.985	3.4
	Arizona	-9.3	0.524	0.986	3.6
	Combined	0.6	0.480	0.982	4.0
	Adjusted	0.1	0.486	0.985	3.8
6	Maryland	1.7	0.447	0.966	4.8
	New York	3.8	0.444	0.969	4.4
	Arizona	-9.1	0.498	0.980	4.2
	Combined	1.9	0.446	0.971	4.8
	Adjusted	1.4	0.453	0.984	4.6
8	Maryland	2.8	0.430	0.952	0.6
	New York	5.3	0.421	0.954	5.1
	Arizona	-6.5	0.473	0.976	4.4
	Combined	3.2	0.427	0.963	5.3
	Adjusted	3.4	0.429	0.965	5.1
10	Maryland	4.0	0.422	0.944	5.8
	New York	6.0	0.415	0.948	5.4
	Arizona	-3.2	0.451	0.972	4.5
	Combined	4.7	0.415	0.958	5.5
	Adjusted	4.4	0.419	0.959	5.4
12	Maryland	5.5	0.413	0.937	6.1
	New York	7.8	0.398	0.937	5.8
	Arizona	-2.3	0.447	0.971	4.5
	Combined	5.8	0.408	0.953	5.7
	Adjusted	5.7	0.411	0.955	5.6

Note: 1 in. = 25 mm.

Table 4. Temperature distributions in asphaltic concrete pavements at 2:00 p.m.

Depth (in.)	Data Set	A	B	R	S.E.
2	Maryland	-2.7	0.574	0.986	4.0
	New York	-3.2	0.595	0.984	4.4
	Arizona	-5.6	0.580	0.992	3.1
	Combined	-1.7	0.569	0.987	4.3
	Adjusted	-2.1	0.576	0.987	4.3
4	Maryland	1.1	0.501	0.987	3.5
	New York	1.4	0.514	0.988	3.4
	Arizona	-7.1	0.539	0.987	3.6
	Combined	1.1	0.503	0.986	3.8
	Adjusted	0.4	0.511	0.989	3.5
6	Maryland	3.6	0.451	0.976	4.2
	New York	4.9	0.452	0.977	4.1
	Arizona	-7.4	0.508	0.983	3.9
	Combined	3.0	0.457	0.979	4.4
	Adjusted	2.1	0.467	0.981	4.2
8	Maryland	5.2	0.422	0.962	5.1
	New York	6.8	0.417	0.961	5.0
	Arizona	-6.9	0.484	0.979	4.1
	Combined	4.4	0.428	0.969	5.0
	Adjusted	4.1	0.433	0.972	4.7
10	Maryland	6.3	0.406	0.950	5.6
	New York	7.9	0.400	0.952	5.3
	Arizona	-5.7	0.466	0.974	4.4
	Combined	5.6	0.410	0.961	5.4
	Adjusted	4.8	0.418	0.963	5.3
12	Maryland	7.4	0.392	0.937	6.2
	New York	10.0	0.375	0.935	5.9
	Arizona	-4.5	0.457	0.973	4.5
	Combined	6.4	0.399	0.953	5.8
	Adjusted	6.0	0.405	0.956	5.6

Note: 1 in. = 25 mm.

ANALYSES AND RESULTS

The same computer program was used to separately analyze the New York and Arizona data sets as was used to analyze the Maryland data set (1). The analyses indicated that a straight-line relationship, $y = A + Bx$, was equally valid for all data sets; however, the equations were not identical (Tables 1 through 6). The major differences among the data sets were in the annual temperature ranges and annual mean temperatures. Inspection of the data and least squares fits showed that, for a given hour, depth, and surface temperature plus 5-day average air temperature history, temperatures differed by as much as 10 F (5.6 C) in the upper (extrapolated) ranges (Figure 1). Closer inspection showed that, when the equation was solved for temperatures within the temperature range for the respective sites, the discrepancies were minimal and generally within the limits of scatter of the Maryland data set.

The scatter (standard error of estimate) for the New York and Arizona data sets was generally less than the scatter for the Maryland data for corresponding depths. However, there were fewer observations. Figure 2 shows the data for 1:00 p.m. and a 4-in. (102-mm) depth. Slight rotational and horizontal shifts were observed in the New York and Arizona data as compared to the Maryland data.

From the standpoint of longitudes, the New York site was 8 clock minutes earlier than the Maryland site; the Arizona site was 16 clock minutes behind the equivalent Maryland clock time. To adjust for these longitudinal effects, New York and Arizona clock times were determined for the appropriate Maryland sun times. Interpolated pavement temperatures for those adjusted clock times were plotted. Figure 3 shows the same data as in Figure 2 but adjusted for longitudinal differences. A threefold net effect of the longitudinal adjustment was noted:

1. The rotational shifts in the fitted straight lines were less,
2. The horizontal shifts between the data sets were less, and
3. Longitudinal adjustments for depths from the surface down to the 2-in. (51-mm) depth were very slight and are likely to be unnecessary [longitudinal adjustments appear to begin to be significant for depths equal to and greater than 4 in. (102 mm)].

The adjustments for longitude resulted in a closer grouping of the data, which fell within the outer limits of the Maryland data. The increased number of observations within the same limits reduces the standard error of estimate and increases the correlation coefficient.

Whether the scatter of pavement temperature data could be reduced by analyzing the data on the basis of daytime exposure to solar radiation was investigated. Analyses were made for sunrise, midmorning, midday, midafternoon, and sunset.

$$\text{Sunrise} = SR$$

$$\text{Midmorning} = SR + 0.25\,(SS - SR)$$

$$\text{Midday} = SR + 0.50\,(SS - SR)$$

$$\text{Midafternoon} = SR + 0.75\,(SS - SR)$$

$$\text{Sunset} = SS$$

where SR = sunrise clock time and SS = sunset clock time, obtained from tables prepared by the Nautical Almanac Office, U. S. Naval Observatory.

After clock times for these five points in time were determined for each day, pavement temperatures were interpolated, recorded, plotted, and analyzed. The results are given in Tables 7 through 11. The scatter of data decreased for the sunrise, midmorning, and sunset times but increased for midday and midafternoon. The wider

Table 5. Temperature distributions in asphaltic concrete pavements at 4:00 p.m.

Depth (in.)	Data Set	A	B	R	S.E.
2	Maryland	-2.7	0.595	0.985	4.4
	New York	-3.7	0.613	0.982	5.0
	Arizona	-0.2	0.577	0.991	3.1
	Combined	-2.1	0.593	0.986	4.5
	Adjusted	-2.8	0.600	0.985	4.6
4	Maryland	2.5	0.526	0.988	3.6
	New York	1.2	0.542	0.987	3.8
	Arizona	0.5	0.544	0.986	3.7
	Combined	1.4	0.537	0.988	3.7
	Adjusted	1.2	0.539	0.989	3.5
6	Maryland	5.8	0.474	0.987	3.4
	New York	4.9	0.482	0.984	3.6
	Arizona	0.0	0.519	0.982	4.1
	Combined	3.8	0.491	0.986	3.7
	Adjusted	3.4	0.496	0.986	3.7
8	Maryland	7.5	0.441	0.981	3.8
	New York	7.1	0.442	0.977	4.0
	Arizona	0.3	0.493	0.978	4.3
	Combined	5.5	0.458	0.980	4.1
	Adjusted	5.3	0.460	0.981	3.9
10	Maryland	8.5	0.420	0.972	4.3
	New York	8.5	0.416	0.970	4.4
	Arizona	1.7	0.468	0.973	4.5
	Combined	6.6	0.434	0.974	4.5
	Adjusted	6.4	0.437	0.973	4.5
12	Maryland	9.9	0.399	0.961	5.0
	New York	10.7	0.386	0.955	5.0
	Arizona	2.6	0.456	0.969	4.7
	Combined	7.7	0.416	0.964	5.1
	Adjusted	7.7	0.417	0.963	5.1

Note: 1 in. = 25 mm.

Table 6. Temperature distributions in asphaltic concrete pavements at 6:00 p.m.

Depth (in.)	Data Set	A	B	R	S.E.
2	Maryland	-5.0	0.619	0.984	4.6
	New York	-3.9	0.621	0.979	5.2
	Arizona	-2.7	0.603	0.989	2.9
	Combined	-4.3	0.618	0.982	4.8
	Adjusted	-4.7	0.619	0.982	4.9
4	Maryland	0.6	0.570	0.985	4.1
	New York	0.2	0.577	0.983	4.3
	Arizona	-0.8	0.594	0.984	3.3
	Combined	0.1	0.577	0.984	4.2
	Adjusted	0.3	0.574	0.985	4.0
6	Maryland	4.9	0.523	0.986	3.6
	New York	3.7	0.531	0.986	3.6
	Arizona	0.0	0.576	0.982	3.5
	Combined	3.7	0.534	0.985	3.7
	Adjusted	3.6	0.532	0.986	3.7
8	Maryland	7.4	0.488	0.986	3.3
	New York	6.0	0.492	0.987	3.2
	Arizona	0.5	0.557	0.980	3.6
	Combined	5.9	0.500	0.985	3.5
	Adjusted	5.9	0.498	0.986	3.4
10	Maryland	8.6	0.465	0.985	3.4
	New York	7.6	0.461	0.986	3.1
	Arizona	1.1	0.538	0.976	3.8
	Combined	7.2	0.474	0.982	3.6
	Adjusted	7.4	0.470	0.982	3.6
12	Maryland	10.2	0.439	0.979	3.7
	New York	9.8	0.429	0.980	3.5
	Arizona	2.7	0.518	0.974	3.8
	Combined	9.0	0.448	0.975	4.0
	Adjusted	9.0	0.444	0.976	4.0

Note: 1 in. = 25 mm.

Figure 1. Temperature at 2-in. (51-mm) depth at 11:00 a.m.

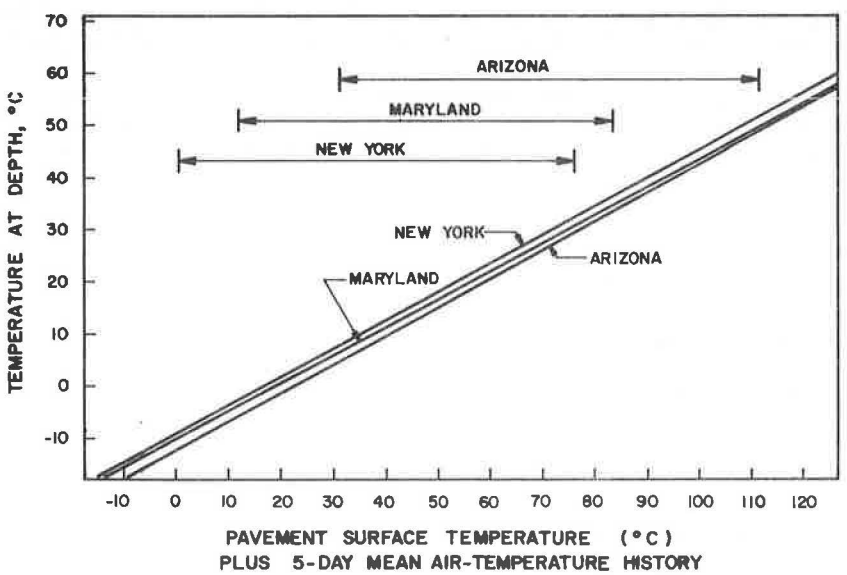

Figure 2. Temperatures at 4-in. (102-mm) depth at 1:00 p.m.

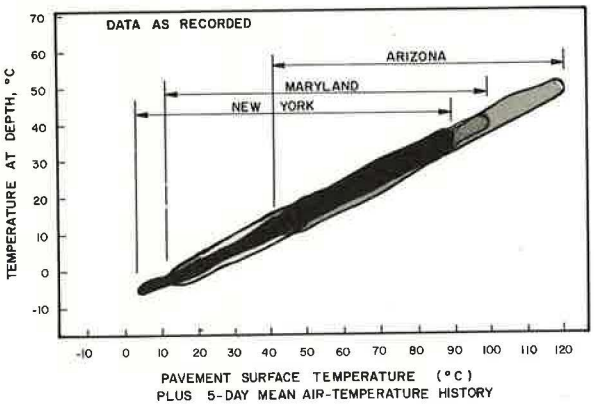

Figure 3. Temperatures at 4-in. (102-mm) depth at 1:00 p.m. adjusted to equivalent Maryland longitude.

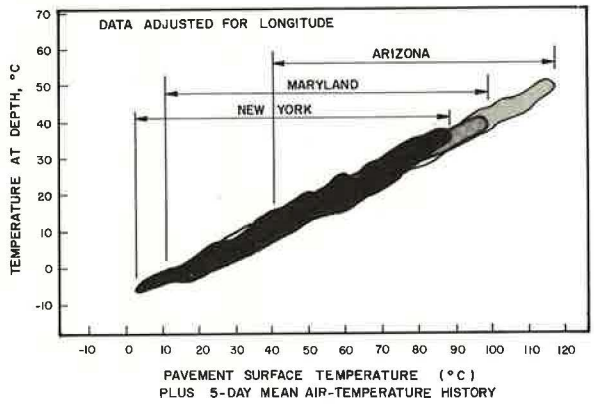

Table 7. Temperature distributions in asphaltic concrete pavements at sunrise.

Depth (in.)	Data Set	A	B	R	S.E.
2	Maryland	-5.2	0.561	0.988	2.8
	New York	-0.7	0.532	0.982	3.1
	Arizona	-2.0	0.534	0.993	2.2
	Combined	-3.1	0.547	0.985	3.0
4	Maryland	-2.8	0.573	0.990	2.6
	New York	-0.3	0.555	0.982	3.3
	Arizona	-0.2	0.546	0.996	1.8
	Combined	-1.5	0.563	0.987	2.9
6	Maryland	-1.7	0.579	0.988	2.9
	New York	0.5	0.565	0.981	3.5
	Arizona	1.4	0.554	0.995	1.8
	Combined	-0.5	0.571	0.986	3.1
8	Maryland	-0.3	0.585	0.987	3.1
	New York	1.4	0.565	0.980	3.6
	Arizona	3.3	0.557	0.994	2.1
	Combined	0.6	0.576	0.985	3.2

Note: 1 in. = 25 mm.

Table 8. Temperature distributions in asphaltic concrete pavements during midmorning.

Depth (in.)	Data Set	A	B	R	S.E.
2	Maryland	-3.1	0.525	0.980	3.3
	New York	-0.1	0.516	0.983	3.0
	Arizona	-6.0	0.544	0.994	2.1
	Combined	-2.0	0.521	0.985	3.1
4	Maryland	-4.4	0.541	0.983	3.2
	New York	-0.8	0.525	0.983	3.1
	Arizona	-5.2	0.530	0.992	2.4
	Combined	-1.6	0.518	0.983	3.3
6	Maryland	-5.2	0.553	0.982	3.4
	New York	-0.7	0.534	0.982	3.2
	Arizona	-4.3	0.529	0.991	2.5
	Combined	-1.6	0.525	0.982	3.5
8	Maryland	-4.5	0.562	0.984	3.3
	New York	-0.3	0.537	0.983	3.1
	Arizona	-2.1	0.526	0.990	2.6
	Combined	-0.9	0.531	0.984	3.4

Note: 1 in. = 25 mm.

Table 9. Temperature distributions in asphaltic concrete pavements during midday.

Depth (in.)	Data Set	A	B	R	S.E.
2	Maryland	-2.4	0.548	0.986	3.7
	New York	-2.7	0.571	0.984	4.0
	Arizona	-6.8	0.563	0.993	2.8
	Combined	-1.3	0.543	0.986	4.0
4	Maryland	0.4	0.482	0.982	3.7
	New York	1.1	0.493	0.984	3.5
	Arizona	-9.9	0.531	0.988	3.5
	Combined	0.4	0.484	0.983	4.0
6	Maryland	1.5	0.451	0.970	4.5
	New York	3.8	0.448	0.972	4.2
	Arizona	-9.7	0.506	0.981	4.1
	Combined	1.7	0.451	0.973	4.7
8	Maryland	2.8	0.434	0.957	5.2
	New York	5.0	0.427	0.960	4.8
	Arizona	-6.1	0.473	0.977	4.3
	Combined	3.4	0.429	0.965	5.1

Note: 1 in. = 25 mm.

Table 10. Temperature distributions in asphaltic concrete pavements during midafternoon.

Depth (in.)	Data Set	A	B	R	S.E.
2	Maryland	-4.9	0.603	0.984	4.6
	New York	-4.5	0.618	0.981	5.1
	Arizona	-5.9	0.599	0.992	3.0
	Combined	-3.4	0.595	0.984	4.7
4	Maryland	-1.4	0.536	0.985	4.0
	New York	-0.8	0.548	0.985	3.9
	Arizona	-8.4	0.574	0.987	3.7
	Combined	-1.4	0.540	0.986	4.1
6	Maryland	0.7	0.491	0.982	3.9
	New York	2.7	0.491	0.982	3.8
	Arizona	-9.3	0.547	0.981	4.2
	Combined	0.4	0.497	0.982	4.2
8	Maryland	2.9	0.458	0.975	4.3
	New York	4.8	0.452	0.974	4.4
	Arizona	-8.1	0.514	0.975	4.6
	Combined	2.6	0.460	0.975	4.6

Note: 1 in. = 25 mm.

Table 11. Temperature distributions in asphaltic concrete pavements at sunset.

Depth (in.)	Data Set	A	B	R	S.E.
2	Maryland	-4.4	0.613	0.979	4.7
	New York	-2.6	0.607	0.972	5.3
	Arizona	-2.6	0.596	0.987	2.8
	Combined	-3.4	0.607	0.977	4.8
4	Maryland	-2.4	0.602	0.983	4.0
	New York	-1.9	0.603	0.977	4.8
	Arizona	-5.7	0.616	0.988	2.7
	Combined	-2.1	0.600	0.981	4.3
6	Maryland	-1.2	0.578	0.985	3.7
	New York	-0.1	0.576	0.981	4.1
	Arizona	-8.1	0.622	0.986	3.0
	Combined	-1.0	0.578	0.983	3.9
8	Maryland	0.0	0.557	0.987	3.3
	New York	1.2	0.548	0.984	3.6
	Arizona	-9.7	0.614	0.983	3.2
	Combined	0.2	0.555	0.985	3.5

Note: 1 in. = 25 mm.

variations at midday and midafternoon may be caused by summer afternoon showers and variable cloud covers. Although this last analysis was of interest and needed to be investigated, the system is very awkward to use, does not provide greater accuracy, and is not recommended for general use. It does, however, lend credence to the original system.

DISCUSSION AND IMPLEMENTATION

Air temperature history adequately accounts for differences in latitude and altitude. Adjustments can be made for differences in longitude by interpolating between hourly graphs, which can be prepared from data given in Tables 1 through 6. If the purpose of estimating pavement temperatures is to determine the magnitude of the asphaltic tensile strain, longitudinal adjustments may well be worth the effort. If the objective is to adjust deflection data (1, 2), such refinements may not be justified. The Asphalt Institute (2) has proposed using one graph for estimating temperatures at various depths to calculate an average pavement temperature that can be used to adjust measured deflections to equivalent deflections at a standard temperature. The discrepancies due to use of one temperature distribution graph are greater than those caused by not adjusting for longitude. Furthermore, the choice of adjustment curves for deflection measurements will have a more pronounced effect than making no adjustment for longitude or exposure to solar radiation. Therefore, the set of equations based on Maryland data (1) may be used with confidence for other latitudes and longitudes.

SUMMARY

1. The addition of a 5-day average air temperature history to the surface temperature results in a straight-line correlation with temperature at a given depth. This relationship appears to be equally valid for data sets from upper New York State, Maryland, and Arizona.
2. The equations originally developed from the Maryland data set appear to be reasonably accurate for other locations.
3. The effects of changes in latitude are accounted for in the air temperature history. The net result is a shift up or down the temperature scale, reflecting the annual temperature range at a particular site.
4. Combining data from Maryland, New York, and Arizona resulted in slightly more scatter than the Maryland set alone.
5. Longitudinally adjusting the New York and Arizona data to equivalent Maryland times reduced the scatter and slightly improved the accuracy.
6. Analyzing all data sets in terms of daytime exposure to solar radiation also resulted in a straight-line correlation between surface temperature plus air temperature history and temperature at a given depth. The graphs for sunrise, midmorning, and sunset were more accurate than the Maryland graphs, whereas those for the midday and midafternoon were less accurate.
7. Analysis of the effect of daytime exposure to solar radiation validated the method of analysis used for the Maryland graphs but is too cumbersome.
8. Graphs derived from the Maryland data are recommended for use in other latitudes and longitudes. More accurate results may be obtained if the clock time at any site is adjusted to a longitude within the time zone equivalent to the College Park, Maryland, longitude of 76° 56' within the Eastern Standard Time zone.

REFERENCES

1. H. F. Southgate and R. C. Deen. Temperature Distribution Within Asphalt Pavements and Its Relationship to Pavement Deflection. Highway Research Record 291, 1969, pp. 116-131.

2. Asphalt Overlays and Pavement Rehabilitation. The Asphalt Institute, Manual Series 17, 1969.
3. B. F. Kallas. Asphalt Pavement Temperatures. Highway Research Record 150, 1966, pp. 1-11.
4. A. L. Straub, H. N. Schenck, Jr., and F. E. Przybycien. Bituminous Pavement Temperature Related to Climate. Highway Research Record 256, 1968, pp. 53-77.
5. T. N. Rumney and R. A. Jimenez. Pavement Temperatures in the Southwest. Highway Research Record 361, 1971, pp. 1-13.

A PRELIMINARY INVESTIGATION OF THE FEASIBILITY OF SPENT OIL SHALE AS ROAD CONSTRUCTION MATERIAL

Gerald J. Gromko, University of Colorado at Denver

The use of spent oil shale material as aggregate for flexible pavement construction was investigated, and its suitability for use both in base courses and in bituminous surface courses is discussed. To assess the aggregate and asphalt-aggregate characteristics of spent shale the following tests were performed: the Los Angeles abrasion test, the dry sieve analysis, the specific gravity test, the Atterberg limits test, and the Hveem method of mix design. The results of the testing showed that the spent shale aggregate was well-graded, flat, angular, highly absorbent, friable, and nonplastic, has a rough surface texture, and wears relatively easily. The aggregate mixes tested by the Hveem stabilometer yielded high strength values and were relatively lightweight. The asphalt-spent shale mixtures studied showed very high total resistance (combination of stability and cohesiometer values) values, i.e., more than adequate load-carrying capability. However, the asphalt contents necessary for these very high strengths were also high. Based on the results of the tests performed, it seems apparent that this particular type of spent shale material might perform very well in flexible pavement structures. Although the material showed more than adequate strength and stability, it may not stand up as well to the abrasive action of traffic on high-capacity roads and may be expensive because of the seemingly large amount of asphalt needed. However, this mixture might perform very well as a surface course layer for lower capacity roads (e.g., secondary roads).

•AS SOURCES of proven aggregates are depleted throughout the country, more use will be made of aggregates that do not have a known service record. A new source of aggregate for Colorado may be the by-products of the oil shale industry. One of the major environmental problems facing this rapidly developing industry is the disposal of enormous amounts of spent shale from the oil extraction processes. Most research in this area has focused on revegetation efforts. However, spent shale has no organic material nor nutrients necessary for the growth of plants. Filling small canyons and other natural depressions with spent shale has also been proposed but has received less than favorable support. In view of this, the use of this material as aggregate for flexible pavement construction was investigated. Tests were performed to determine the suitability of one particular type of spent shale aggregate for possible use as base course material or in bituminous surface courses. Successful results could lead to an economic solution for both the processors of the raw oil shale and the users (construction agencies) of the seeming waste, spent shale.

Publication of this paper sponsored by Committee on Characteristics of Bituminous-Aggregate Combinations to Meet Surface Requirements.

CHARACTERISTICS AND PROPERTIES OF SPENT SHALE

Generally, raw oil shale is a fine-grained, compact sedimentary marlstone, which may consist of dolomite, quartz, clay, calcite, and other minerals and which contains an organic substance called kerogen. Kerogen is only slightly soluble in known petroleum solvents but is readily converted to shale oil when subjected to temperatures between 700 and 950 F (371 and 510 C). As each particle of kerogen in the raw oil shale reaches its decomposition temperature in the retorting process, it vaporizes, leaving a void area in the shale. As heat continues to penetrate the shale, successive kerogen particles are vaporized and escape from the shale through pore spaces previously occupied with kerogen. The vapors are then condensed to yield the crude shale oil.

The spent shale is the solid waste remaining after retorting and other processing have removed hydrocarbon values and possibly associated mineral values from raw oil shale (1). The spent shale varies in particle size and chemical properties depending on the grade of raw oil shale and type of processing method used (2). Spent shale can range in size from a very fine ash (minus No. 200 sieve) to relatively large chunks (9 in., 229 mm, or more). The chemical analysis of Fischer assay spent shales obtained from raw Colorado oil shale samples is given in Table 1 (3). The constituents of burned shale are as follows:

Constituent	Average Percentage
SiO_2	43.8
Fe_2O_3	4.6
Al_2O_3	12.2
CaO	22.1
MgO	9.3
SO_3	2.2
Na_2O	3.4
K_2O	2.4

Except, perhaps, for its particle size, spent shale from the Fischer assay is generally representative of spent shale from any indirect heated retorting process.

In Table 2, Dinneen (4, 5) has reported the compressive strength of core samples of Green River oil shale before and after retorting. Samples of raw oil shale displayed high compressive strengths whether determined perpendicular or parallel to the bedding planes of the shale. After heating to 950 F (510 C), the lean spent oil shale retained relatively high compressive strength values in both horizontal and vertical planes, indicating a high degree of inorganic cementation between the mineral particles making up each lamina and between adjacent laminae. It is also evident from Table 2 that the compressive strength of rich (high oil yield) spent oil shale is quite low after the organic matter (kerogen) is removed.

A study (6) conducted by the Denver Research Institute (DRI) in 1966 discussed the disposal and uses of spent shale ash (material passing No. 200 sieve). A significant result of this study was the development of cohesion in the shale ash, when it was subjected to burning temperatures from 1,150 to 1,700 F (521 to 927 C) and burning times from ½ sec to 2 hours, and the resulting high compressive strengths of the shale ash test specimens. However, most processing methods are conducted with burning temperatures ranging from 700 to 950 F (371 to 510 C), resulting in spent shale that is nonplastic and noncohesive, e.g., the material investigated by the author. Another DRI study (7) on spent oil shale ash showed that this material can possibly be used as fines in asphaltic concrete, as a soil-cement additive for road base and subbase material, and as lightweight aggregate for highway use.

Other researches (8, 9, 10) have obtained data on spent shale (particle size ranging from plus No. 4 through minus No. 200 sieves, with the majority passing the No. 200

sieve) in the form of compaction characteristics, Atterberg limits, consolidation, and triaxial characteristics. Their conclusions (10) are given below.

1. The spent shale material loses strength significantly upon saturation. For partially saturated spent shales (moisture content between 5 and 20 percent), the strength increases with an increase in dry densities. However, upon saturation, the strength seems to be independent of magnitude of dry densities in the range tested.
2. The angle of internal friction of saturated spent shales is on the order of 20 deg; that for the partially saturated spent shales was 35 deg.

These relatively high angles of internal friction usually indicate a material that may exhibit a relatively high frictional component of shear strength (a characteristic that is very desirable in flexible pavement structures).

It is readily apparent from this discussion that much of the research reported to data has concentrated on so-called spent shale ash material. This research has shown that this material does possess some of the desirable characteristics of the more traditional forms of aggregate in construction use. However, the use of large quantities of material with such small particle sizes and limited particle size range is not very practical for large construction operations, e.g., earth embankments, and flexible pavements. Little if any research has been conducted on larger sizes and a wider range of sizes of spent shale. Consequently, the remainder of this paper is devoted to an evaluation of a limited number of physical characteristics of relatively coarser material (with only 10 percent of it, classified as ash, passing the No. 200 sieve).

EVALUATION AND DISCUSSION OF SPENT SHALE AGGREGATE AND MIXES

Methodology

The spent shale investigated in this study was obtained from the U.S. Bureau of Mines, Laramie Energy Research Center (LERC), in Wyoming. The raw oil shale in use at LERC originated from the Green River formation in which the Colorado shale field is located (11). The retorting process in use at LERC is the Nevada-Texas-Utah (NTU) process, which uses very large pieces of raw oil shale. Approximately 20 percent of the raw oil shale used is larger than 20 in. (508 mm) in size. Some typical chemical properties of the spent shale from the NTU retort at LERC are given in Table 3 (12).

To evaluate the suitability of this material for use in road construction, the following tests were performed with the cooperation of the Materials Division of the Colorado Division of Highways (CDH): the Los Angeles abrasion test, dry sieve analysis, specific gravity, Atterberg limits, and the Hveem method of mix design. These tests were used to determine the following aggregate characteristics: size and grading, toughness, particle shape, surface texture, absorption, and affinity for asphalt. These basic aggregate characteristics combine to yield the desirable properties that asphalt-aggregate and aggregate mixes must possess to perform satisfactorily as pavement mixtures. The desirable properties of pavement mixtures (13) include stability, durability, flexibility, fatigue resistance, skid resistance, impermeability, and workability.

Size, Grading, and Atterberg Limits

The material received from LERC ranged in size from approximately 9 in. (229 mm) to less than 0.0029 in. (0.07 mm, minus No. 200 sieve); the majority was less than 1 in. (25 mm). For convenience in handling, the material was passed through a small rock crusher set at a maximum size of $\frac{3}{4}$ in. (19 mm) before the dry sieve analysis was performed. The gradation curve shown in Figure 1 conforms to the Asphalt Institute's type 4-B (14) and CDH's E grading for asphalt-concrete surface course mixtures. This

Table 1. Chemical analyses of spent shales from Fischer assays conducted on Colorado oil shale samples.

Constituents	Grade of Original Oil Shale Sample						
	17.8	19.5	22.3	29.8	36.6	38.0	51.8
Carbon (total)	7.26	7.62	8.56	8.12	10.27	10.07	10.32
Carbon (organic)	1.81	1.69	2.49	2.57	3.53	4.20	4.55
Hydrogen	0.26	0.22	0.15	0.24	0.27	0.22	0.26
Nitrogen	0.11	0.10	0.18	0.21	0.24	0.27	0.33
Sulfur	0.37	0.29	0.50	0.61	0.47	0.66	1.06

Table 2. Compressive strengths of raw and thermally treated oil shales (in psi).

Oil Yield (liters/ metric ton)	Raw Oil Shales		Oil Shale Heated to 510 C		Oil Shale Heated to 816 C	
	A	B	A	B	A	B
4.2	22,168	19,382	19,979	19,084	15,469	14,892
27.1	31,177	28,377	28,178	26,175	17,080	13,585
56.3	26,573	23,375	13,286	6,196	10,487	3,695
104.3	16,388	18,587	412	384	171	156
125.2	9,890	10,586	355	284	114	114
164.8	11,496	13,770	71	114	85	114
244.1	12,988	2,889	28	28	57	28

Note: A = compressive strength perpendicular to the bedding planes; B = compressive strength parallel to the bedding planes. 1 psi = 6900 Pa.

Table 3. Properties of spent shale.

Shale Analysis	Experiment																	
	1	2	3	4	5	6	7	8	9	10	11	12	13	14	15	16	17	18
Fischer assay Oil, gal/ton	16.2	7.6	4.92	0.1	0	0.3	0.8	0	0	1.2	1.31	0	0	0	0	0.95	0.3	0
Oil, wt percent	6.2	2.9	1.81	0.05	0	0.1	0.32	0	0	0.47	0	0	0	0	0	0.38	0.1	0
Water, gal/ ton	1.3	1.1	0.63	0.9	0.8	1.9	2.0	0.08	0	1.7	0.38	0.2	1.1	1.4	1.4	0.5	2.2	0.8
Hydrogen, wt percent	1.17	0.56	0.51	0.15	0.14	0.14	0.34	0.11	0.06	0.31	0.24	0.14	0.18	0.22	0.17	0.23	0.20	0.14
Carbon Total wt percent	13.23	8.78	8.04	4.87	4.99	5.53	5.14	4.04	2.85	6.34	5.36	4.00	6.02	7.12	4.33	7.19	2.41	3.62
Mineral wt percent	5.02	4.76	2.99	3.20	3.34	3.46	3.09	2.70	1.13	3.40	2.52	2.67	4.05	3.99	2.86	3.48	1.59	2.19
Organic wt percent	8.21	4.02	5.05	1.67	1.65	2.07	2.05	1.34	1.70	2.94	2.83	1.33	1.97	3.14	1.46	3.71	0.82	1.43
Carbon dioxide, wt percent	18.39	17.46	10.97	11.73	12.27	12.67	11.14	9.88	3.72	12.46	9.26	9.77	14.83	14.61	10.49	12.12	5.84	8.02
Ash, wt percent	71.71	77.46	83.69	86.87	87.30	84.33	85.82	88.77	95.61	83.04	88.34	88.67	82.91	82.29	87.62	83.95	92.82	90.61
Nitrogen, wt percent	0.32	0.17	0.21	0.12	0.12	0.10	0.12	0.09	0.06	0.19	0.13	0.08	0.12	0.14	0.08	0.21	0.08	0.09
Sulfur, wt percent	0.52	0.54	0.97	1.28	0.93	0.56	0.75	0.94	0.86	0.60	0.82	0.66	0.70	0.67	0.73	0.82	0.98	0.74
Mineral carbon dioxide, wt percent	25.08	23.81	14.96	15.99	16.73	17.27	15.19	13.47	4.88	16.99	12.63	13.32	20.22	19.92	14.30	16.49	7.96	10.94
Water soluble carbonates, wt percent	0.23	1.21	4.53	3.43	2.21	0.95	0.99	1.40	3.88	1.23	2.09	0	1.82	0.22	1.31	1.14	1.44	1.40
Water soluble bicarbonates, wt percent	0.32	0.17	0.23	0.07	0.94	0.08	0.07	0.08	0.11	0.07	0.06	1.60	0.08	0.52	0.74	0.07	0.08	0.12
Heat value, Btu/lb (gross)	1,490	610	490	90	150	300	170	40	160	300	380	140	160	410	70	500	70	140

Note: 1 gal/ton = 3800/907 cm^3/kg; 1 Btu/lb = 2326 J/kg.

Figure 1. Gradation curve for spent shale aggregate.

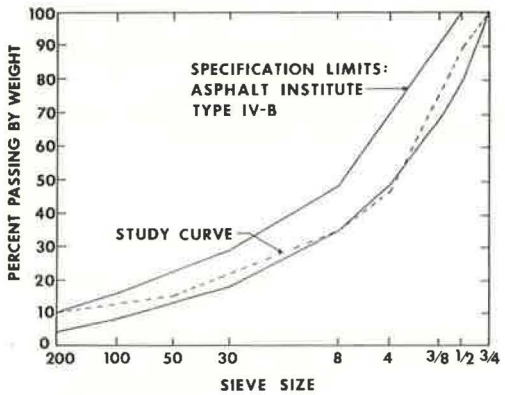

Table 4. Hveem test results.

Percent Bitumen	Specific Gravity of Specimen	Stability Value	Cohesiometer Value	R_t
11	1.831	39	199	98
12	1.851	36	284	100
13*	1.896	18	276	86
14	1.884	–	174	–

*Maximum specific gravity of 1.950, and voids in compacted specimen of 2.7 percent.

gradation can be described as a relatively dense, well-graded, aggregate blend that should exhibit high strength characteristics.

The Atterberg limits tests (liquid and plastic limits) were performed on a portion of the material passing the No. 40 sieve. The results from these tests showed that the material was nonplastic and thus noncohesive.

Toughness

The Los Angeles abrasion test was conducted to determine the toughness or the abrasion resistance of the spent shale particles. The wear was 48.5 percent. This is slightly higher than the maximum allowable limit (45 percent) reported in the CDH standard specifications. Consequently, this material may not stand up so well as tougher aggregates (such as traprock) to the repeated abrasive action of traffic. Therefore, the spent shale particles should probably be used in the lower pavement layers (binder, base, and subbase courses).

Particle Shape and Surface Texture

Particles retained on the No. 50 sieve are dark gray, friable, flat, angular, and sharp-cornered and have a relatively rough surface texture. Microscopic examination of smaller sizes (minus No. 200) similar to those of this study was reported by Heley and Terrel (8), who found that

1. The particles were crystalline and bulky;
2. Individual particles varied in size, and the larger particles were created by a fusion together of many smaller particles; and
3. The particles are not honeycombed in structure, but large amalgamations do contain many interstices that, because of their fused structure, are possibly isolated from surface fluids.

These characteristics are typical of aggregates that result in relatively high angles (35 to 45 deg) of internal friction. Although a determination of this angle was not performed for the material from LERC, recent research (10) indicates that this angle for spent shale ash can vary from 20 deg for saturated triaxial specimens to 35 deg for partially saturated specimens [moisture contents ranging from 5 to 20 percent and dry densities from 85 to 95 lb/ft^3 (1360 to 1520 kg/m^3)].

Absorption

The centrifuge kerosene equivalent (CKE) test was performed on the spent shale aggregate to determine the estimated oil ratio to use for the subsequent Hveem mixtures. Both the kerosene and oil used to determine the degree of absorption showed a relatively high percentage of porosity; approximately 15 percent of each (kerosene and oil) was retained. The probable reason for this high porosity is the high temperatures used in the retorting process on the raw oil shale as mentioned previously. This characteristic will more than likely necessitate adding an extra amount of asphalt to the paving mix to satisfy the aggregates' seemingly high absorption capacity.

Affinity for Asphalt

Stripping, the separation of asphalt film from the aggregate through the action of water, may make an aggregate unsuitable for asphalt paving mixtures. Immersion-compression tests were performed on asphalt-spent shale mixtures containing 13 percent asphalt. The results were as follows:

Item	Value
Wet strength, psi	359
Dry strength, psi	357
Percentage of absorption by weight	1.36
Percentage of swell by volume	0.00
Index of retained strength	100

These results show a negligible loss of strength, indicating that the spent shale exhibits very high resistance to stripping.

Strength of Spent Shale Aggregate Mixtures

In general, soil strength depends on density, moisture content, and texture of the soil (15). The Hveem stabilometer test was performed to evaluate the shear strength (frictional component) of typically prepared spent shale aggregate specimens.

The stabilometer R-value, expressing the measure of a soil or aggregate's ability to resist the transmission of vertical load in a lateral or horizontal direction, was determined for moist spent shale aggregate specimens and was found to be 85 (average of three tests, all of which were the same value). The associated density and moisture content were 93 lb/ft^3 (1488 kg/m^3) and 18.1 percent. The main reasons for this high strength have been previously discussed. An R-value of 85 significantly exceeds the minimum value of 78 (16) for aggregate base course layers. This indicates that use of spent shale as conventional base course material should be highly recommended. Because of its relatively high strength, more of this material could be used to provide thicker base course layers, probably resulting in thinner asphalt-concrete surface courses for many roads.

In summary, the spent shale is well graded yielding dense mixtures; is flat, angular, and of rough surface texture yielding a relatively high angle of internal friction and therefore high strength in compaction specimens; exhibits very high resistance to stripping; and is a highly absorbent and friable material that appears to wear relatively easily.

Hveem Asphalt-Spent Shale Mixtures

The Hveem method of mix design, typically used to determine the probable optimum asphalt content for pavement mixtures, was used to evaluate the suitability of asphalt-spent shale mixtures. The principal features of this method are (13) the CKE test on the aggregates, a stabilometer test, a cohesiometer test, a swell test, and a density-voids analysis on compacted paving mixtures. The CKE test was performed on samples of spent shale (both plus No. 4 and minus No. 4 sieve sizes) to determine the estimated optimum asphalt content, which was 14 percent. Four Hveem samples ranging in asphalt content from 11 to 14 percent were then made. The results given in Table 4 indicate some interesting characteristics. First, it appears that the optimum asphalt content for maximum stability is slightly greater than 11 percent. This at first seems high when compared to a more normal value of 6 percent for most surface course mixes. However, when the specific gravities of spent shale and normal aggregate are compared (1.85 versus 2.35 respectively) the seemingly high asphalt content of 11 percent for the spent shale aggregate is equivalent to 9 percent for normal aggregate. Second, the total resistance value R_t (combination of stability and cohesiometer value) of approximately 100 is surprisingly high. This seems to indicate that the asphalt-spent shale mix possesses very high strength, i.e., more than adequate load-carrying capability.

It is evident from the results shown in Table 4 that the mixtures investigated possess extremely high stability. This is due to dense aggregate gradation, angular shape, and

rough surface texture, all of which contribute to a high angle of internal friction and thus to a high frictional component of shear strength, and a relatively high value of cohesion exhibited by the mixture.

Only a partial evaluation can be made at this time of mixture durability, its ability to resist disintegration from weathering and traffic. The results from the Los Angeles abrasion test show that the spent-shale itself may not stand up so well to the repeated abrasive action of traffic. The soundness test, which provides an indication of the resistance to weathering of aggregate, was not performed. Traditionally, however, the shale type of material is unsound because water enters it and, upon freezing, expands and fractures it (14). Hence, based on this limited information the spent shale probably should not be used for surface course paving mixtures.

Because of the limited testing, the property of flexibility cannot be fully assessed. This property is, however, enhanced by high asphalt contents and relatively open-graded aggregates. The asphalt contents tested were high, but the gradation was dense. Because the spent shale is highly absorbent, it is not known how much of the asphalt is absorbed nor how much effectively coats the aggregate. This question might be resolved in a future study.

Fatigue resistance is also enhanced by high asphalt contents and well-graded aggregates. The mixes studied conform to these criteria; consequently, they might exhibit more than adequate fatigue resistance.

The cohesiometer test determines the cohesion properties and the tensile strength of asphalt films. The cohesiometer values obtained in this investigation, near the estimated optimum, are relatively high and substantially exceed the minimum values reported by most design criteria (13). The higher the tensile strength is, the greater are the properties of flexibility and fatigue resistance. Thus, with the relatively high cohesiometer values obtained, it seems likely that the asphalt-spent shale mix might possess more than adequate flexibility and fatigue resistance.

The same factors that govern high stability usually apply to high skid resistance. From the preliminary testing conducted, it seems likely that the spent shale does possess the rough surface texture and angular particle shape necessary for adequate skid resistance.

The results from the immersion-compression test provide an excellent indication of the relative impermeability of the asphalt-spent shale mixture. The absorption of water by weight was slightly greater than 1 percent. This indicates that the mix used is relatively dense graded and impermeable.

Visual examination revealed that the asphalt-spent shale mixtures were difficult to mix. The problem of adequate workability in the field, however, cannot accurately be assessed at this time. This also might be considered in a future investigation.

Although the asphalt-spent shale mixtures possess many of the desirable properties discussed above, its use as a surface layer for high types of roads is questionable. However, these mixtures might perform very well in surface courses for lightly traveled roads (e.g., secondary roads). It seems more likely that these mixtures might be highly beneficial for use in binder layers and also in bituminous base layers.

RECOMMENDATIONS AND CONCLUSIONS

Even though this investigation was very limited in scope, it indicates the suitability of this particular type of spent shale for use in binder layer, bituminous base, conventional base, or subbase layers for flexible pavements. Although the spent shale showed more than adequate strength and stability, its use as aggregate for asphalt concrete surface course mixtures may be dependent on the traffic characteristics of the road involved. Field installations using this material would have to be constructed to evaluate the performance of this material more completely.

Based on the results of the tests performed, the following conclusions are made.

1. Spent shale can be described as bulky, angular, rough, and highly absorptive material capable of producing very high strength, relatively lightweight aggregate mixtures.

2. Asphalt-spent shale mixtures tested by the Hveem method show that very high strengths can be obtained with this material. However, the asphalt contents required to produce these strengths are high.
3. The results of stabilometer tests on aggregate mixtures also indicated very high strengths, pointing to the possible use of this material for base and subbase courses.
4. Based on this limited investigation, this particular type of spent shale material might perform very well in flexible pavement structures.

ACKNOWLEDGMENTS

The experimental work for this study was performed by the staff of the Materials Division of the Colorado Division of Highways, Denver. Their assistance in this effort is greatly appreciated. Special appreciation is expressed to Bud A. Brakey, Chief Materials Engineer, for his cooperation and critical review of this paper.

REFERENCES

1. T. A. Hendrickson. The Properties of Spent Shale. Unpublished report of Cameron Engineers, 1974.
2. T. A. Hendrickson. Oil Shale Processing Methods. Proc., Seventh Oil Shale Symposium, Colorado School of Mines, Vol. 69, No. 2, April 1974.
3. K. E. Stanfield. Properties of Colorado Oil Shale. U.S. Bureau of Mines, Rept. of Investigations 4825, 1951.
4. G. U. Dinneen et al. Constitution of Green River Oil Shale. Presented at the United Nations Symposium on the Development and Utilization of Oil Shale Resources, Tallinn, Estonia, 1968.
5. G. U. Dinneen. Oil Shale and the Energy Crisis. Presented at ASME Annual Meeting, New York, 1972.
6. W. J. Culbertson and T. D. Nevens. Uses of Spent Oil Shale Ash. Denver Research Institute, Univ. of Denver, Aug. 21, 1972.
7. T. D. Nevens et al. Disposal and Uses of Oil Shale Ash. Denver Research Institute Rept. 2546, 1970.
8. W. Heley and L. R. Terrel. Processed Shale Embankment Study. Colony Development Operation, Atlantic Richfield Co., Dec. 1971.
9. Liquefaction Studies: Proposed Processed Shale Disposal Pile, Parachute Creek, Colorado. Dames and Moore Consulting Engineers in the Earth Sciences, Sept. 1971.
10. Slope Stability Studies: Proposed Processed Shale Embankment, Parachute Creek, Colorado. Dames and Moore Consulting Engineers in the Earth Sciences, Nov. 1971.
11. J. R. Donnell. Geology and Oil-Shale Resources of the Green River Formation. First Annual Symposium on Oil Shale, pp. 153-163.
12. H. C. Carpenter and H. W. Sohns. Application of Aboveground Retorting Variables to In-Situ Oil Shale Processing. Proc., First Five Oil Shale Symposiums, 1964-1968.
13. Mix Design Methods for Asphalt Concrete and Other Hot-Mix Types. The Asphalt Institute, Manual Series 2, Third Ed., Oct. 1969.
14. Asphalt Technology and Construction Instructor's Guide. The Asphalt Institute, ES-1, Jan. 1971.
15. E. J. Yoder. Principles of Pavement Design. John Wiley and Sons, 1959.
16. Roadway Design Manual. Division of Highways, Colorado Department of Highways, Jan. 1972.

DESIGN CONSIDERATIONS FOR A DIRECT-FIRED PROPANE HEATER TO PREHEAT THE BASE FOR COLD-WEATHER PAVING

N. D. Shah and P. F. Dickson, Colorado School of Mines, Golden

A prototype direct-fired propane heater with variable gas rate and speed was designed for preheating the base to study cold-weather paving of thin mats. The results obtained were compared with those predicted by the computer program. The computer program was then used to simulate cold-weather paving. Statistical analysis of the data revealed that only three of the eight variables were significant. The effect of these three significant variables on the time available for compaction was found to be linear. A nomogram was constructed to predict the time available for compaction. From the results of this study, a 12 by 12-ft (3.6 by 3.6-m) propane heater producing approximately 300,000 Btu/hr-ft^2 (9300 kW/m^2) and moving 2 min ahead of the paver at a speed of 20 to 80 ft/min (6.1 to 24 m/min) is recommended as a final design. Propane gas consumption for such a heater is estimated to be 1,980 lb/hr (890 kg/h), which will result in a fuel cost of $138/hr.

•COLD-WEATHER paving of a thin mat is hampered by rapid cooling. Preheating the base is one method to retard this rapid cooling, and theoretical and practical aspects of base preheating have been studied (1, 2).

This study was undertaken to design a variable-speed propane heater to preheat the base before the thin mat is placed. The results of laboratory experiments were compared with those predicted by the computer program developed by Corlew and Dickson (2). The principal objective of the study was to determine the effect of some of the variables on the time available for compaction. The ultimate goal was to design a propane heater that could be used in real practice.

Laboratory experiments have been conducted in which test specimens of asphalt base were preheated with a direct-fired propane heater. These experiments were restricted to preheating and subsequent cooling of the base. Placing of thin mat on a preheated base was not considered. The capacity of the experimental heater was 90,000 Btu/hr-ft^2 (279 kW/m^2). The heater was stationary, which is impractical because the openings for the burner and air intake could not be changed, which made it impossible to adjust the flame. In the present study, most of these problems were overcome, and the laboratory experiments investigated base preheating and the placing of thin mat on the preheated base.

EXPERIMENTATION

The experimental setup is shown in Figure 1. The direct-fired propane heater was fueled from a 100-lb (45-kg) liquefied petroleum gas (LPG) tank. The gas flow rates were controlled by needle valves installed in the gas line just before the flow meter.

Publication of this paper sponsored by Committee on Flexible Pavement Construction.

Figure 1. Experimental setup for base preheating.

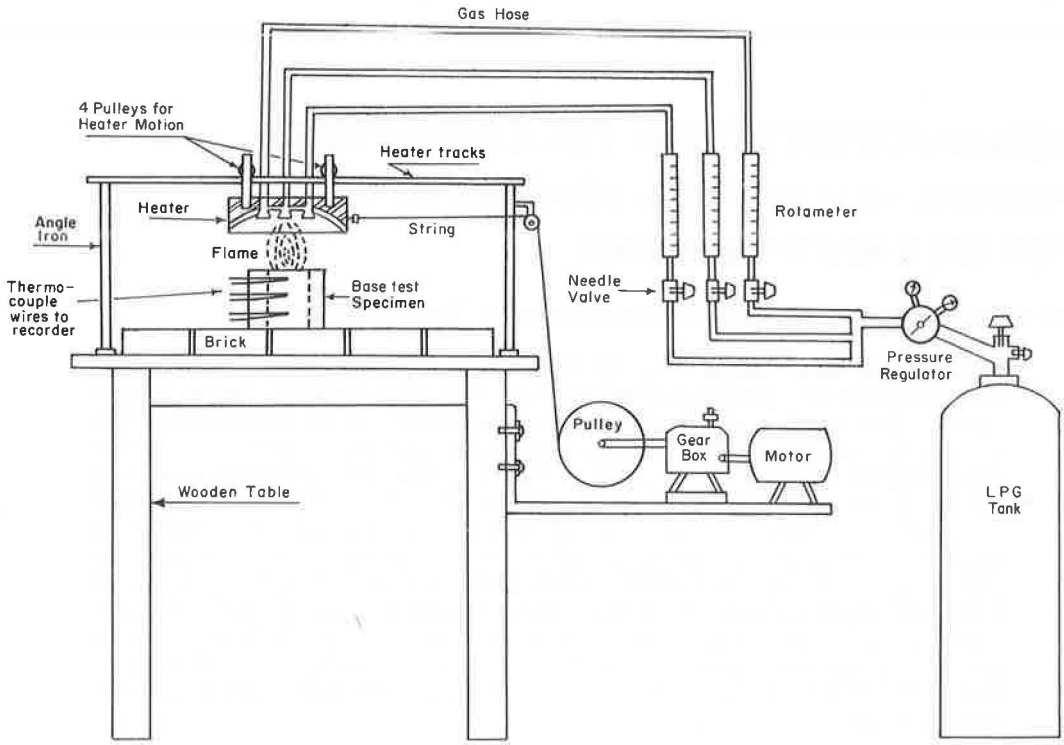

Figure 2. Burner design.

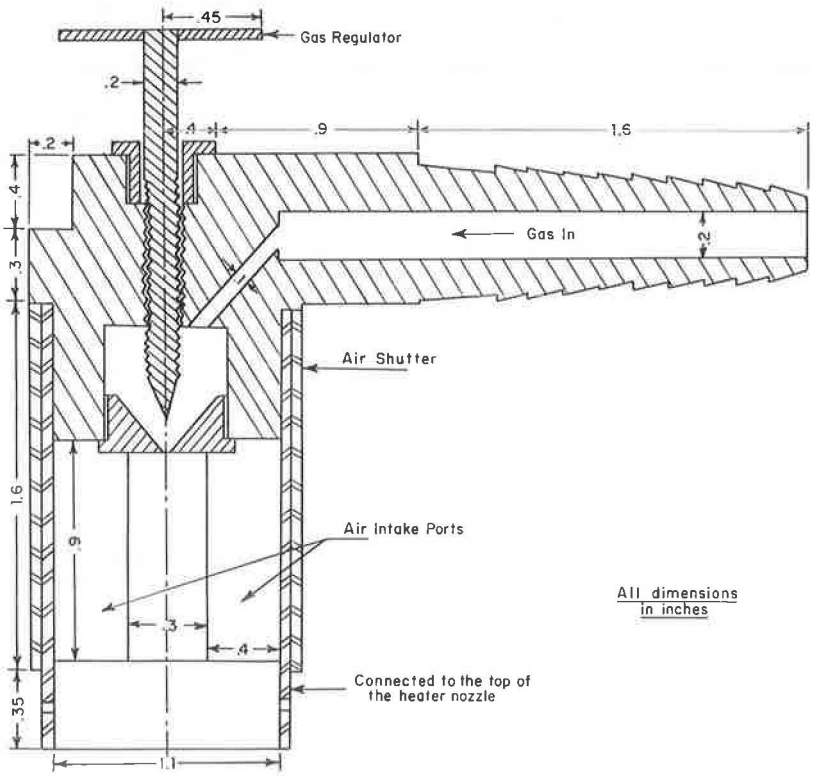

The gas was supplied from the flow meter to the variable-opening orifice of the burner. The burner design (Figure 2) was similar to the conventional Bunsen burner. The entire heater with four pulleys was mounted on two tracks, which were supported at both ends by angle irons. The heater was connected with a thick cotton string to a 6-in.-diameter (152-mm) pulley, which was driven by a ¼-hp (186-W), 1,725-rpm motor through a gear box. The lowest speed that could be obtained by using the gear box was 4 ft/min (0.02 m/s).

A detailed design of the heater is shown in Figure 3. The heater shell was made from 1/16-in.-thick (1.6-mm) stainless steel 303 sheets. The top inner half of the heater was filled with asbestos paste to avoid heat loss. The heater was lined with ¼-in.-thick (6.4-mm) refractory, which was held in place by 14 anchors. The entire heater weighed approximately 10 lb (4.5 kg). The distance between the heater and the base specimen could be adjusted by raising or lowering the base specimen.

The experimental procedure mainly consisted of the following four steps:

1. Preheating the cold base specimen by moving the propane heater above it at a desired speed,
2. Cooling the base specimen during the stall period,
3. Placing the thin hot-mixed asphalt specimen on the base, and
4. Cooling the thin mat specimen from 300 to 150 F (149 to 66 C) on the preheated base.

During this period all the temperatures were recorded as a function of time on a 24-channel Acco Bristol recorder.

COMPARISON OF EXPERIMENTAL AND COMPUTED RESULTS

Nine experimental runs were made by using different combinations of heat output, mat thickness, preheat time, and initial base and mat temperature values. Comparison of experimental temperatures with computed temperatures for a few typical runs is shown in Figures 4, 5, and 6. Comparisons of only upper base points and all the points in the mat are given. The temperature changes below a certain depth in the base are insignificant during the preheating and stall periods. That is why the comparison at the point 1 in. (25 mm) from the top in the base is not given during preheating and the stall period. Also the comparison for the interfacial temperature is not given during these periods because of the experimental difficulties encountered in accurately measuring it.

In Figure 4, computed results are shown for 10, 20, and 40 percent heat losses. The computed temperature profile does not significantly change; hence, the effect of heat loss is probably insignificant. The same conclusion will be reached later on the basis of systematic statistical study of the variables.

Figures 4 and 5 show that there is a considerable difference between the experimental and computed results. However, in all cases mat cooling was slower for the experimental results than for computed results. This apparent disparity between the experimental and computed results could be due to existence of a thin layer of air between the two samples. The layer of air between the samples acts as an insulation, which retards the cooling of thin mat. For the run shown in Figure 6, the thin mat specimen was hammered periodically after it was placed on the preheated base specimen. The close contact between the hammered samples resulted in greater agreement between experimental and computed results.

To quantitatively explain the effect of a thin layer of air between two samples, the computer program was modified to take into account this resistance. Computer runs were made with 0, 1/80, 1/40, and 1/20-in.-thick (0.3, 0.6, and 1.2-mm) layers of air between samples, and it was found that 1/40 in. (0.6 mm) of air gave good agreement between the experimental and computed results. The results in Figure 5 show that the agreement between the experimental and modified computed result is considerably improved.

Figure 3. Detailed design of heater.

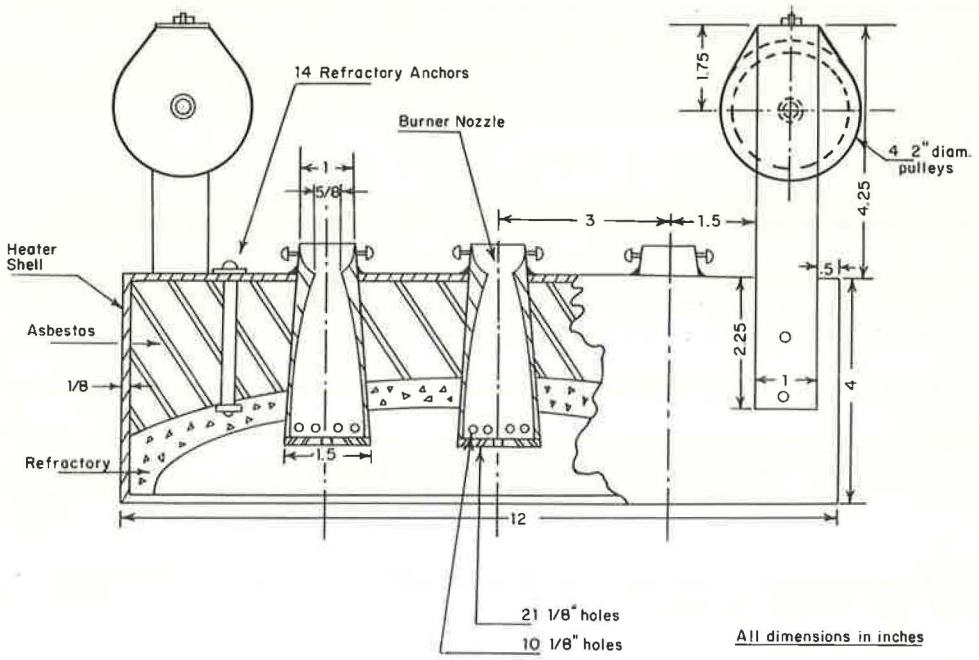

Figure 4. Comparison of experimental results and computed results for 10, 20, and 40 percent heat losses.

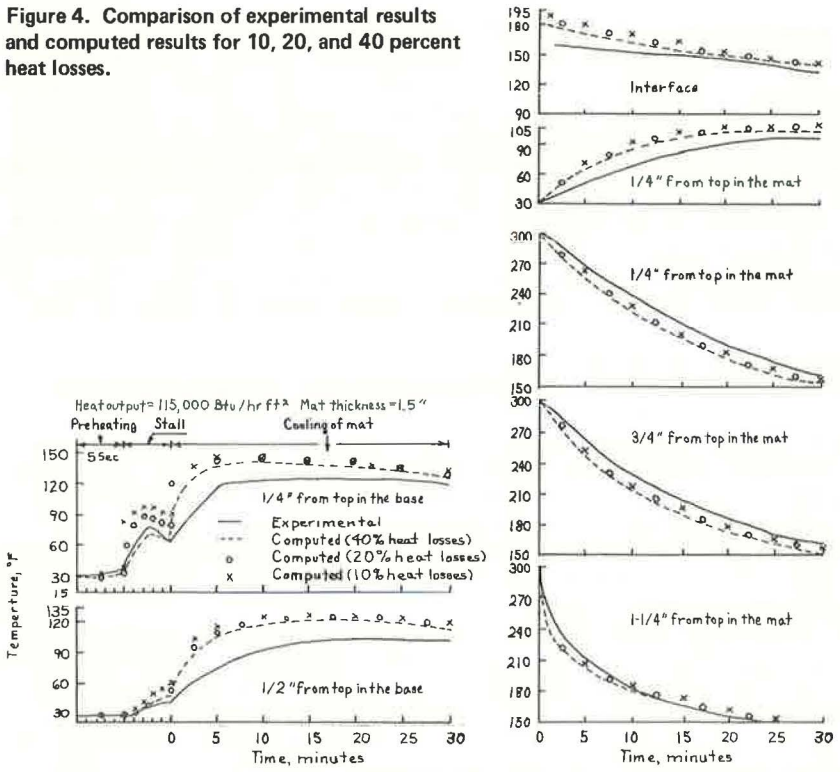

Figure 5. Comparison of experimental results and computed results, including $^1/_{40}$-in. (0.6-mm) air layer.

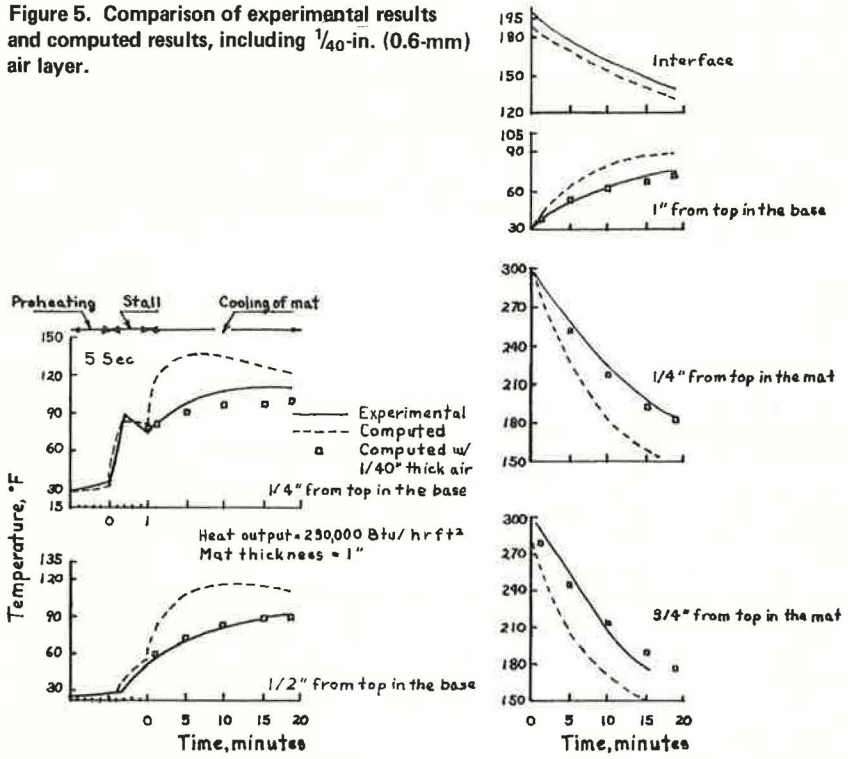

Figure 6. Comparison of experimental and computed results for hammered samples.

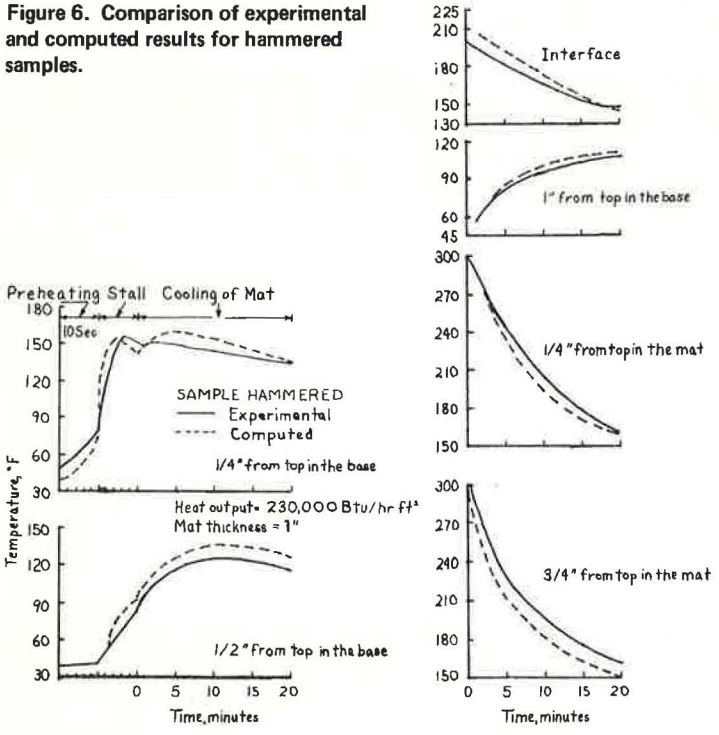

SIMULATED COLD-WEATHER PAVING

The computer program developed by Corlew and Dickson (2) was used to simulate cold-weather paving. For the purpose of preliminary study, eight variables were investigated at two levels each (Table 1). The dependent variable was time to cool to 175 or 150 F (79.4 and 66 C). Initially 16 computer runs were selected. The detailed statistical analysis for these 16 runs, together with confounding of some interactions, is given by Shah (3). The following factors were found to be significant at the 5 percent level (in decreasing order of importance):

1. Mat thickness,
2. Wind velocity, and
3. Preheat time.

The results were the same for time to cool to both 175 and 150 F. None of the second-order interactions was found to be significant.

Mat thickness and wind velocity were found to be the most significant variables. The same conclusion was reached by Shah and Dickson (4) in their study on use of insulation in cold-weather paving. Surprisingly heat output was not found to be significant; however, a close examination would reveal that heat output is connected with preheat time, and in this case preheat time is significant.

Stall period is not significant, which means that we can be flexible in setting the distance between the heater and paver. Initial base temperature or atmospheric temperature is not significant, which means that minor changes or fluctuations in the environmental temperature would not appreciably change the design conditions. We can be flexible in designing the heater capacity because heat losses and heat ouput are not significant. Small changes in lay-down temperature do not significantly affect the time available for compaction. Preheat time is found to be significant, and, depending on the preheat time required, the heater speed should be adjusted. To synchronize the various operations requires that the heater and paver move at nearly the same speed. It should be remembered that these conclusions are strictly valid within the range of the variables studied.

Based on the results of this analysis, 48 more computer runs were made. For these runs preheat times of 9, 18, 27, and 36 sec; mat thicknesses of $\frac{1}{2}$, 1, and $1\frac{1}{2}$ in. (12.5, 25, and 38 mm); and wind velocities of 0, 5, 10, and 15 mph (8, 16, and 24 km/h) were used. These data were utilized to find a relationship among time to cool to 175 or 150 F (79.4 or 66 C) and three significant variables by using a step-wise multiple linear regression program. The relationships were

$$\text{Time (150)} = 18.01\,(A) - 0.80\,(B) + 0.39\,(C) - 2.33 \quad (1)$$

$$\text{Time (175)} = 12.88\,(A) - 0.54\,(B) + 0.30\,(C) - 2.64 \quad (2)$$

where time is in min and

A = mat thickness in in. (mm),
B = wind velocity in mph (km/h), and
C = preheat time in sec.

A nomogram (Figure 7) was constructed to obtain the time available for compaction by a graphical procedure. Point G on the scale of mat thickness is joined by a straight line to point H on preheat time scale. Point I, which is the intersection of line GH with scale A, is joined by another straight line to point K on the wind velocity scale. Point J, which is the intersection of line IK with the time scale, gives the time available for compaction.

Table 1. Variables used in computer simulation.

Factor	Symbol	High Value	Low Value
Mat thickness, in.	X_1	1.5	0.5
Wind velocity, mph	X_2	15	0
Preheat time, sec	X_3	36	9
Stall time, min	X_4	3	1
Initial mat temperature, F	X_5	300	250
Initial base temperature, F	X_6	40	10
Heat loss, percent	X_7	40	20
Heat output, Btu/hr-ft^2	X_8	443,000	148,000

Note: 1 in. = 25 mm; 1 mph = 1.6 km/h; 1 F = 1.8 C + 32; 1 Btu/hr-ft^2 = 3.1 W/m^2.

Table 2. Base preheating versus insulation in cold-weather paving.

Mat Thickness (in.)	Preheat Time (sec)	Insulation Thickness (in.)	Time to 175 F (min)	Time to 150 F (min)
0.5	0	0	1.5	2.8
	9	—	2.7	4.7
	18	—	4.5	6.8
	27	—	6.1	9.0
	36	—	8.1	11.3
	—	1/16	5.0	6.8
	—	1/8	6.0	7.8
	—	1/4	7.0	8.7
1.0	0	0	5.5	8.3
	9	—	7.3	10.7
	18	—	9.7	13.7
	27	—	12	16.6
	36	—	14.3	19.2
	—	1/16	11	14.8
	—	1/8	12.8	15.9
	—	1/4	14.3	18.9

Note: 1 in. = 25 mm; 1 F = 1.8 C + 32.

Figure 7. Nomogram for base preheating.

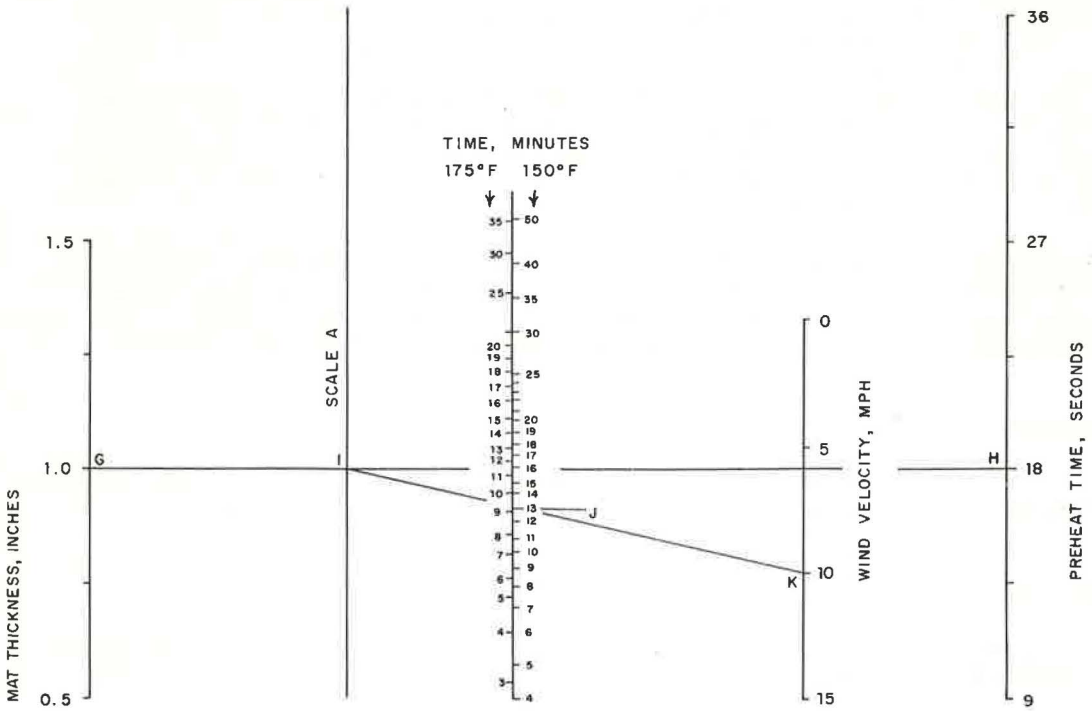

Based on the results of this study and other data (4), a comparison of base preheating and insulation is given in Table 2. All data were obtained for 25 F (-3.8 C) base temperature and 10-mph (16-km/h) wind velocity. Based on heat transfer considerations, both methods seem to be equally attractive and efficient. However, from practical consideration, base preheating seems to be the more useful method.

From the results of this study, recommendations regarding the final design of the heater could be made. The breadth of the heater should be the same as the breadth of the paver. The length of the heater depends on preheat time required and the speed at which it is moving. Assuming paver speeds of 20 to 80 ft/min (6.1 to 24 m/min) in normal operations (5), a 12-ft-long (3.6-m) heater will give 36 to 9 sec of preheat time depending on the speed. Thus a 12 by 12-ft propane heater producing approximately 300,000 Btu/hr-ft^2 (9300 kW/m^2) and moving 2 min ahead of pavers at a speed between 20 and 80 ft/min could be recommended. Depending on the speed, the distance between the heater and paver would be between 40 and 160 ft (12 and 48 m). It is further recommended that the heater be designed so that the vertical distance between the burner and base surface can be changed as desired. The LPG consumption for such a heater is estimated to be 1,980 lb/hr (890 kg/h). The estimated fuel cost for LPG would be $138/hr based on the cost of LPG at $7/100 lb ($7/45 kg).

CONCLUSIONS

The results of this study suggest that a direct-fired, refractory-lined propane heater can be effectively used for base preheating to achieve adequate time for compaction of thin mats. Base preheating is the most useful method from practical considerations, even in the face of today's energy shortage.

The experimental results establish the validity of the mathematical model for predicting base preheating and cooling of mat. Statistical analysis showed that mat thickness, wind velocity, and preheat time are significant variables affecting the time available for compaction. The relationship among time available for compaction and these three variables is linear within the range of the variables studied.

A 12 by 12-ft (3.6 by 3.6-m) propane heater with approximately 300,000-Btu/hr-ft^2 (9300-kW/m^2) capacity is needed to achieve adequate time for compaction of thin mats. The heater should move 40 to 160 ft (12 to 48 m) ahead of pavers at a speed between 20 and 80 ft/min (6.1 and 24 m/min) depending on the preheat time required. The propane gas consumption would be 1,980 lb/hr (890 kg/h) at a fuel cost of $138/hr.

ACKNOWLEDGEMENT

The authors wish to express their sincere thanks for the support of the National Science Foundation, who made this research possible.

REFERENCES

1. B. G. Frenzel, P. F. Dickson, and J. S. Corlew. Computer Analysis for Modification of Base Environmental Conditions to Permit Cold Weather Paving. Proc., AAPT, Vol. 40, 1971, pp. 487-508.
2. J. S. Corlew and P. F. Dickson. Cold Weather Paving of Thin Lifts of Hot-Mixed Asphalt on Preheated Asphalt Base. Highway Research Record 385, 1972.
3. N. D. Shah. Cooling of Hot-Mix Asphalt Laid on an Insulated or Preheated Base. Colorado School of Mines, PhD thesis, 1973.
4. N. D. Shah and P. F. Dickson. Cooling of Hot-Mixed Asphalt Laid on an Insulated Base. HRB Special Rept. 148, 1974.
5. J. S. Corlew. Thermal Energy Transport in Asphalt Paving Operations With Base Preheat. Colorado School of Mines, PhD thesis, 1971.

SPONSORSHIP OF THIS RECORD

GROUP 2—DESIGN AND CONSTRUCTION OF TRANSPORTATION FACILITIES
W. B. Drake, Kentucky Department of Transportation, chairman

BITUMINOUS SECTION
Moreland Herrin, University of Illinois at Champaign-Urbana, chairman

Committee on Characteristics of Bituminous-Aggregate Combinations to Meet Surface Requirements
Kamran Majidzadeh, Ohio State University, chairman
Sabir H. Dahir, Rudolf A. Jimenez, Charles A. Pagen, James M. Rice, James A. Scherocman, R. J. Schmidt, Stewart R. Spelman, E. A. Whitehurst, Frank M. Williams

Committee on Characteristics of Bituminous Paving Mixtures to Meet Structural Requirements
Donald R. Schwartz, Illinois Department of Transportation, chairman
David A. Anderson, Charles W. Beagle, H. W. Busching, James A. Cechetini, J. T. Corkill, Jon A. Epps, Oren S. Fletcher, Charles R. Foster, William J. Harper, R. G. Hicks, Rudolf A. Jimenez, Ignat V. Kalcheff, Bernard F. Kallas, Carl L. Monismith, Charles V. Owen, Charles F. Parker, David W. Rand, R. M. Ripple, Byron E. Ruth, Paul J. Serafin, Jack E. Stephens, Ronald L. Terrel, David G. Tunnicliff, Thomas D. White

CONSTRUCTION SECTION
Robert D. Schmidt, Illinois Department of Transportation, chairman

Committee on Flexible Pavement Construction
W. E. Latham, North Carolina Department of Transportation and Highway Safety, chairman
Verdi Adam, Charles W. Beagle, R. W. Beaty, Larue Delp, Frank M. Drake, Jon A. Epps, Charles R. Foster, G. F. Kemper, Duncan A. McCrae, Charles F. Parker, David W. Rand, Orrin Riley, Vernon L. Schrimper, W. H. Shaw, R. R. Stander, Gerald S. Triplett, David G. Tunnicliff, Lansing Tuttle, P. J. White

William G. Gunderman, Transportation Research Board staff

Sponsorship is indicated by a footnote on the first page of each report. The organizational units and the chairmen and members are as of December 31, 1974.